

## Towards autonomous photogrammetric forest inventory using a lightweight under-canopy robotic drone

Väinö Karjalainen<sup>a,\*</sup>, Niko Koivumäki<sup>a,\*</sup>, Teemu Hakala<sup>a</sup>, Jesse Muhojoki<sup>a</sup>, Eric Hyypä<sup>a</sup>, Anand George<sup>a</sup>, Juha Suomalainen<sup>a</sup>, Eija Honkavaara<sup>a</sup>

<sup>a</sup>Department of Remote Sensing and Photogrammetry, Finnish Geospatial Research Institute FGI, The National Land Survey of Finland

### ARTICLE HISTORY

Compiled July 4, 2025

### ABSTRACT

Drones are increasingly used in forestry to capture high-resolution remote sensing data, supporting enhanced monitoring, assessment, and decision-making processes. While operations above the forest canopy are already highly automated, flying inside forests remains challenging, primarily relying on manual piloting. Inside dense forests, reliance on the Global Navigation Satellite System (GNSS) for localization is not feasible. Additionally, the drone must autonomously adjust its flight path to avoid collisions. Recently, advancements in robotics have enabled autonomous drone flights in GNSS-denied obstacle-rich areas. In this article, a step towards autonomous forest data collection is taken by building a prototype of a robotic under-canopy drone utilizing state-of-the-art open-source methods and validating its performance for data collection inside forests. Specifically, the study focused on camera-based autonomous flight under the forest canopy and photogrammetric post-processing of the data collected with the low-cost onboard stereo camera. The autonomous flight capability of the prototype was evaluated through multiple test flights at boreal forests. The tree parameter estimation capability was studied by performing diameter at breast height (DBH) estimation. The prototype successfully carried out flights in selected challenging forest environments, and the experiments showed excellent performance in forest 3D modeling with a miniaturized stereoscopic photogrammetric system. The DBH estimation achieved a root mean square error (RMSE) of 3.33 cm (12.79 %) across all trees. For trees with a DBH less than 30 cm, the RMSE was 1.16 cm (5.74 %). The results provide valuable insights into autonomous under-canopy forest mapping and highlight the critical next steps for advancing lightweight robotic drone systems for mapping complex forest environments.

### KEYWORDS

Robotic; drone; forest; photogrammetry; DBH

## 1. Introduction

Over the last decades, remote sensing measurements within forests have been increasingly used to capture detailed forest information. Terrestrial laser scanning (TLS) made a breakthrough in the early 2000s, followed by the development of various solutions, including static laser scanning using tripods (Bienert et al. 2007) and mobile solutions, e.g., handheld devices (Ryding et al. 2015; Bauwens et al. 2016; Marselis et al. 2016; Balenović et al. 2021), backpacks (Liang et al. 2014b, 2018; Hyypä et al. 2020b),

---

\* Authors contributed equally. CONTACT Väinö Karjalainen. Email: vaino.karjalainen@nls.fi

ground-based vehicles (Forsman, Holmgren, and Olofsson 2016; Liang et al. 2018; Bienenert et al. 2018) or drones (Chisholm et al. 2013; Brede et al. 2017; Wieser et al. 2017; Hyyppä et al. 2020a). Similarly, the use of structure-from-motion (SFM) based point clouds for forest mapping has been demonstrated using different camera solutions (e.g., Liang et al. 2014a; Wallace et al. 2016; Kuželka and Surový 2018; Piermattei et al. 2019). Among these methods, drone-based solutions offer several benefits, including the ability to move in areas with challenging terrain and the high potential for automatization.

Hence, the use of drones in forestry research has rapidly increased, and they offer a practical solution for forest data collection above the forest canopy (Puliti et al. 2015; Tuominen et al. 2017). Modern commercial drones are highly automated and can execute data collection missions highly autonomously in open-air environments using autopilot systems. However, their positioning systems typically rely exclusively on GNSS signals, limiting autonomous flights to open areas where these signals are reliable. In dense forests, GNSS localization becomes unreliable due to signal blockages and multipath effects caused by trees (Schubert et al. 2010). Additionally, navigating inside forests requires the capability to autonomously avoid obstacles such as trees and bushes along the flight path. Consequently, drone data collection flights under the forest canopy are still primarily controlled manually by human pilots (e.g., Hyyppä et al. 2020a; Liang et al. 2019; Krisanski, Taskhiri, and Turner 2020; Prabhu et al. 2024).

Recent advances in robotics and the enhanced computational capabilities of small embedded computers have enabled drone autonomy even in GNSS-denied, cluttered environments. Although technology is still in the early stage of development, some recent studies have proposed various methods that have been successfully tested in forest environments (e.g., Liu et al. 2022; Loquercio et al. 2021; Zhou et al. 2022). However, the proposed methods are typically validated by reporting a single successful test flight in a specific forest environment. Most studies assess the effects of varying object density only in simulators, with only a couple of the methods tested through multiple test flights inside real forests.

Moreover, most of the studies proposing methods for autonomous under-canopy drone trajectory planning have the scope solely on aerial robotics, and the sensor data is primarily utilized only for navigation. Only a few pioneering studies have yet explored the potential of custom robotic under-canopy drone systems in forestry applications (Liu et al. 2022; Liang et al. 2024; Cheng et al. 2024). Notably, all of these studies have utilized Ouster OS1 3D LiDAR (Ouster, San Francisco, CA, USA) as the main sensor. Whereas LiDARs have their strengths, such as 360° horizontal field of view (FOV), long sensing range, and robustness against varying illumination, they tend to be heavier and have higher power consumption than cameras (Reddy Cenkeramaddi et al. 2020). In the case of drone development, where optimizing the weight and battery consumption play a key role, these factors lead to bigger and heavier drone platforms and flight batteries requiring more space between the obstacles to fly safely inside the forest. Moreover, LiDARs with suitable quality are more expensive than camera systems with built-in 3D imaging capability, leading to increased building cost. The data collected with the LiDARs is also limited to point clouds only, whereas the images collected with cameras can also be used for image-based analysis.

Hence, although some LiDAR-based robotic drone systems have been successfully applied to under-canopy mapping of forest parameters, the potential of smaller and cheaper camera-based systems remains largely unexplored. Furthermore, the robotic drone systems proposed in the literature are typically not evaluated through multiple flight tests in different forest environments leaving the reliability and suitability to diverse forest environments as an open question.

Therefore, in this study, a prototype of a small camera-based robotic drone system that can fly autonomously in challenging GNSS-denied forests was built and developed using custom hardware and state-of-the-art robotic methods. The study aimed to tackle the research gaps in flight reliability of camera-based robotic drone systems in various boreal forest environments, as well as the potential of photogrammetric DBH estimation with autonomous drones in such environments. The performance and the reliability of autonomous flight capabilities were evaluated by performing multiple test flights in boreal forests with varying difficulty. In addition, the image data collected with the low-cost onboard stereo camera were processed into point clouds, and the DBH values were estimated for the trees detected from the dataset. To the best of our knowledge, this study is the first to empirically validate a miniaturized, autonomous, camera-based robotic drone for under-canopy forest reconstruction.

Specifically, the study focused on three research questions. What level of autonomous flight reliability can be achieved in challenging boreal forests with current methods for camera-based robotic drone navigation? What level of DBH estimation accuracy can be achieved with the low-cost onboard stereo-camera data recorded during the flight? What are the remaining bottlenecks to be tackled in follow-up studies in order to achieve large-scale autonomous photogrammetric forest data collecting with miniaturized under-canopy robotic drone systems?

The main contributions of this study can be highlighted as follows:

- Build and development of a lightweight robotic drone prototype capable of flying within GNSS-denied forest environments, using custom hardware and state-of-the-art robotic algorithms. The reliability of the system was comprehensively evaluated through multiple test flights in boreal forests with varying tree densities and difficulty levels.
- Combining autonomous flight capabilities to under-canopy photogrammetric forest reconstruction by processing the data from a low-cost onboard stereo-camera to 3D point clouds.
- Validation of autonomous flight data collection based on stereo cameras for the estimation of forest parameters through DBH estimation, including an evaluation of the impact of various factors on the accuracy of the estimate.
- Comprehensive discussion of current limitations to large-scale, fully autonomous photogrammetric under-canopy forest monitoring, along with proposed solutions and further research directions.

The rest of this study is structured as follows. Section 2 reviews the latest studies that estimate DBH using drones flying inside forests and recent open-source solutions for autonomous drone flights inside forests. Section 3 describes the algorithms, hardware, experiments, and methods utilized in this study. Experimental results are presented in Section 4. Section 5 discusses the results, and potential improvements, and concludes the study.

## 2. Related work

### 2.1. *DBH estimation from under-canopy drone data*

In a forest inventory, DBH is one of the most important attributes to estimate, as it provides a measure of the size of a tree and enables the prediction of the total stem volume either alone or combined with the tree height (Laasasenaho 1982). Although

some of the relevant studies have also estimated tree volume by flying the flight path multiple times with different altitudes, with rotating sensors, or with Lidars with high vertical FOV, only DBH estimation accuracies and methods are included in this brief literature review.

In the existing literature, LiDAR-based methods have been studied extensively for the purpose of efficiently and accurately estimating various tree attributes, such as DBH, tree height, and stem volume. To date, several LiDAR-based mobile platforms have been shown to enable DBH estimation of individual trees with an RMSE of 1-2 cm (Ryding et al. 2015; Bauwens et al. 2016; Cabo et al. 2018; Chen et al. 2019; Hyypä et al. 2020b,a, 2022), though most studies have focused on relatively sparse forests with little understory vegetation.

Chisholm et al. (2013) were the first to demonstrate DBH measurements from point cloud data collected with a manually piloted drone flying under the forest canopy. The utilized custom-built drone system included Hokuyo UTM-30LX 2D LiDAR (Hokuyo, Osaka, Japan). They detected 12 trees in the vicinity of the drone trajectory and reported an RMSE of 25.1 % for the DBH estimates of the detected trees.

Hyypä et al. (2020a) collected high-quality point cloud data using a Kaarta Stencil-1 (Kaarta, Pittsburgh, Pennsylvania, USA) laser scanner mounted horizontally at the bottom of a manually piloted drone. They demonstrated DBH estimates with an RMSE of 0.69-0.92 cm (2.2 %-3.1 %) and a bias of 0.29-0.31 cm (1.0 %-1.1 %) on two plots of varying complexity in a boreal forest with a tree density of 410-420 trees/ha. Importantly, their stem diameter estimation algorithm utilized the temporal order of data points to detect stem arcs, thus mitigating distortions caused by slow temporal drifts of the drone trajectory. In a follow-up study, Hyypä et al. (2020c) compared various mobile laser-scanning methods, including backpack, handheld, Under-Canopy UAV, and Above-Canopy UAV, for forest data collection. The same manually piloted under-canopy drone system was utilized in this study in the same forest plots as in Hyypä et al. (2020a). In this study, the manually piloted under-canopy drone system yielded an RMSE of 0.6-1.1 cm (2.3 %-3.5 %) and a bias of 0.34-0.12 cm (1.3 %-0.4 %). Wang et al. (2021) combined data from above- and under-canopy flights of a manually-piloted drone, resulting in an RMSE of 7.95 cm (33.35 %) and a bias of 3.72 cm (15.61 %) for the DBH.

Muhojoki et al. (2024) compared the accuracy of the estimated tree attributes from several LiDAR-based mobile systems, including two under-canopy drone systems, a system by Hovermap (2020 version, Emesent, Milton, Australia) equipped with a Velodyne VLP-16 laser scanner (Velodyne Lidar, San Jose, CA, USA) and a system by Deep Forestry (Deep Forestry, Uppsala, Sweden) utilizing an Ouster OS0-32 Rev. 5 laser scanner (Ouster, San Francisco, CA, USA). Deep Forestry drone was flown manually, but the Hovermap drone system was able to fly autonomously in sparse forests where the distance between the trees was at least 3 m. Both drone systems were used to collect point clouds under the canopy of three sparse forest plots. The RMSE and bias of DBH estimates for Deep Forestry and Hovermap drones, with bias removal method introduced by Muhojoki et al. (2024), averaged RMSE of 1.5 cm (6.7 %) and bias of -0.7 cm (3.0 %) and RMSE of 1.6 cm (6.9 %) and bias of -0.1 cm (-0.6 %), respectively. Without using the bias removal method, RMSE and bias for both drones were significantly higher.

In addition to the manually controlled drones and large autonomous commercial drone systems, recently a few pioneering studies have applied smaller custom robotic drone platforms with a high automation level for LiDAR-based under-canopy DBH estimation. Liang et al. (2024) applied an autonomously operated under-canopy drone

system to collect laser scanning data inside a 50 m  $\times$  30 m forest plot with a tree density of approximately 1000 trees/ha. To enable autonomous flight, a predefined global path was planned, to which the drone system performed real-time adjustments during the flight according to real-time environmental conditions. When the flight path covered most of the test plot, they achieved an RMSE of 5.13 cm (22.01 %) and bias of 3.40 cm (14.62 %) for the DBH of individual trees.

Liu et al. (2022) employed a LiDAR-based semantic lidar odometry and mapping framework (SLOAM) (Chen et al. 2020) algorithm to calculate the number of trees in the explored area. Although in this study the autonomous flight was demonstrated without the SLOAM algorithm and the tree number calculation was only demonstrated with one manually-piloted test flight, the same drone system has later been used in various follow-up studies for tree parameter estimation. Prabhu et al. (2024) extended the system to have 3D trajectory planning capability and used the platform to demonstrate metric-semantic map merging between multiple robotic drones as well as DBH and tree trunk diameter profile estimation with the onboard LiDAR data. The DBH values were estimated for 20 trees located in two different test plots with RMSE of 1.67 cm (7.42 %). However, the DBH data-collecting flights were performed with manual flight mode. Cheng et al. (2024) used the same drone platform to collect a dataset for LiDAR-based mapping of trees. In addition to data from orchards, the dataset contains the onboard LiDAR data from two forest areas. Although the drone was manually piloted in one of these forests, the data collection at the other forest consisting of loblolly pine trees was performed in autonomous flight mode. They also estimated the DBH value for 77 trees from the LiDAR data collected during the autonomous flights achieving an RMSE of 3.8 cm (12.3 %) by offline afterprocessing and 9.8 cm (31.8 %) by online estimation with SLOAM. With manually piloted data collection in the second test forest consisting of 20 trees with varying species, the RMSEs were 2.0 cm (7.5 %) with offline processing and 7.5 cm (27.5 %) with online processing.

Besides the under-canopy flying drones, LiDARs have also been integrated to above-canopy flying drones capable of direct stem diameter measurements, though typically with a significantly higher RMSE and a lower tree detection rate due to the larger measurement distance and the upper canopy obstructing the tree stems (Wieser et al. 2017; Brede et al. 2017; Kuželka, Slavík, and Surový 2020; Vandendaele et al. 2021; Feng et al. 2022).

During the past decade, photogrammetric systems producing SfM point clouds have been suggested to provide an efficient, low-cost alternative to traditional field measurements of tree attributes, such as DBH. Even though several studies have investigated terrestrial photogrammetric systems (e.g., Liang et al. (2014a); Surový, Yoshimoto, and Panagiotidis (2016); Mokroš et al. (2018); Piermattei et al. (2019); Xu, Shen, and Cao (2023); Gao and Kan (2022)) and above-canopy photogrammetric systems (e.g., Wallace et al. (2016); Ye, van Leeuwen, and Nyktas (2019)) for tree attribute estimation, only relatively few studies have tested the use of under-canopy drone systems for the collection of SfM point clouds enabling tree attribute measurements (Kuželka and Surový 2018; Krisanski, Taskhiri, and Turner 2020; Shimabuku, Konoshima, and Ota 2023; He et al. 2025).

Kuželka and Surový (2018) manually operated a drone system based on a DJI Phantom 4 Pro (DJI, Shenzhen, China) within two forest plots to produce low-noise photogrammetric point clouds, from which the DBH of individual trees could be estimated with an RMSE between 2.6 cm and 5.3 cm depending on the plot and the applied analysis method. The studied plots were sparse with only 270-290 trees/ha. Krisanski, Taskhiri, and Turner (2020) performed manual flights with a DJI Phantom 4 Pro in-

side two forest plots with a stem density of approximately 1000 trees/ha to acquire high-density SfM point cloud data, from which the DBH of individual trees could be measured with an RMSE of 1.1-2.1 cm.

Shimabuku, Konoshima, and Ota (2023) achieved an RMSE of 0.4-0.7 cm for DBH estimation on two small subtropical forest plots using SfM point clouds acquired with an under-canopy flying DJI Mini 3 Pro drone (DJI, Shenzhen, China). The first plot containing 18 trees was clean containing a minimal amount of low-hanging branches and understory vegetation. The second test plot was denser and closer to a natural subtropical forest environment but contained only 7 trees. The drone system was able to detect obstacles in the horizontal direction but needed manual piloting to avoid obstacles in the vertical direction and to guide the drone back to the intended flight path after automatic obstacle avoidance in the horizontal direction.

Recently, He et al. (2025) mounted an additional 360° FOV Insta360 camera (Arashi Vision, Shenzhen, China) to the same LiDAR-based autonomous drone platform used in Liu et al. (2022) and post-processed the photogrammetric data to 3D point clouds. Whether the flights were performed in autonomous flight mode or with manually piloted mode was not mentioned in the study. Their study evaluated DBH for 43 trees with varying tree species and the reported median relative DBH error was 11.5 % estimated from the photogrammetric point clouds.

A summary of the results obtained in the relevant studies on under-canopy forest inventory is presented in Table 1. In summary of the related work, most of the studies for under-canopy drone-based DBH estimation have been performed with manually piloted drones. Although a few studies have explored the potential of custom robotic drone systems capable of flying without commands from the pilot during the flight, all of these systems have been based on LiDARs. All of the studies based on photogrammetry and SfM point clouds have utilized commercial drone systems, which have required manual piloting during the data collection.

The highest estimation accuracies have been obtained with large systems unable to fly in dense forests or with test plots containing very few reference trees, but miniaturized systems have still yielded promising results. Notably, all studies utilizing SfM point clouds have been performed in environments that differ significantly from boreal forests.

## ***2.2. Autonomous flying inside forests***

Even though only a few studies have yet utilized robotic under-canopy drones in DBH estimation, drone autonomy itself has been an actively researched topic in the robotics community during the past few years. Recent advances in mobile robotics and the enhanced computational capabilities of small embedded computers have made it realistic to build drones capable of real-time trajectory planning in GNSS-denied cluttered environments. Although technology is still in the early stage of development, some recent studies have proposed various methods that have been successfully tested in forest environments. Most importantly, the authors of these methods have also shared their source code to be openly available for the research community to encourage more development in the field. While the methods utilize various sensor setups, they can be divided into LiDAR-based methods (Liu et al. 2022; Prabhu et al. 2024; Ren et al. 2022; Liu, Ren, and Zhang 2024; Ahmad et al. 2022) and camera-based methods (Campos-Macías et al. 2021; Zhou et al. 2022; Loquercio et al. 2021; Nguyen et al. 2023) based on the sensor utilized for the sensing of the obstacles in the flight path. Since GNSS is not a suitable method for localization under the forest canopy, these methods rely on various Simul-

Table 1.: Accuracy of the stem diameter breast height (DBH) estimations in other studies. SfM-MVS: Structure-from-motion and multi-view stereo; ULS: Under canopy laser scanning; ALS: Above canopy laser scanning. \*averaged values from three plots. The study by He et al. (2025) was omitted from this table since they reported only median errors instead of RMSE.

Dataset	Type	Number of trees	RMSE (cm)	RMSE %	Bias (cm)	Bias %
Chisholm et al. (2013)	ULS	12	-	25.1	-	-
Liang et al. (2024) traj. I	ULS	143	9.79	61.41	7.18	45.03
Liang et al. (2024) traj. II	ULS	143	5.13	22.01	3.40	14.62
Hyypä et al. (2020a) plot I	ULS	42	0.69	2.2	0.31	1.1
Hyypä et al. (2020a) plot II	ULS	43	0.92	3.1	0.29	1.0
Hyypä et al. (2020c) plot I	ULS	42	0.6	2.3	0.34	1.3
Hyypä et al. (2020c) plot II	ULS	43	1.1	3.5	0.12	0.4
Wang et al. (2021)	ULS&ALS	-	7.95	33.35	3.72	15.61
Muhojoki et al.* (2024)	ULS	50	1.50-1.60	6.70-6.90	0.10-0.70	0.60-3.00
Prabhu et al. (2024)	ULS	20	1.67	7.42	-	-
Cheng et al. (2024) Plot I	ULS	77	3.8	12.8	-	-
Cheng et al. (2024) Plot II	ULS	20	2.0	7.5	-	-
Shimabuku et al. (2023) plot I	Drone SfM-MVS	18	0.7	3.6	-	-
Shimabuku et al. (2023) plot II	Drone SfM-MVS	7	0.4	3.2	-	-
Kuželka and Surový (2018)	Drone SfM-MVS	119	2.63-5.31	7.01-13.3	0.27-3.77	0.69-10.11
Krisanski et al. (2020)	Drone SfM-MVS	29	4.1	-	-	-

taneous localization and mapping (SLAM) or odometry algorithms and onboard sensor data to obtain the pose estimate in a local coordinate system. Most of these methods tackle the problem of collision-free trajectory planning using 3D grid maps, but the solutions by Loquercio et al. (2021) and Nguyen et al. (2023) replaced individual mapping and trajectory planning subtasks by deep neural networks mapping the depth images directly to collision-free trajectories. In addition, the methods proposed by Zhou et al. (2022) and Ahmad et al. (2022) concentrated a swarm of drones instead of autonomous flying of an individual drone.

However, most of these methods are typically validated by a single successful autonomous test flight in a specific forest environment. Only four of the articles reported multiple test flights inside real forests (Loquercio et al. 2021; Ren et al. 2022; Liu, Ren, and Zhang 2024; Prabhu et al. 2024). From these, (Loquercio et al. 2021) and (Prabhu et al. 2024) were the only methods tested at least in two different forest types. Moreover, since methods by (Loquercio et al. 2021), (Ren et al. 2022), and (Liu, Ren, and Zhang 2024) were all targeting high-speed flight, the test forests reported in those studies were relatively sparse, with a low amount of low-hanging branches and understory vegetation. The autonomous trajectory planning method by Prabhu et al. (2024) was

also tested only in environments where the space between the trees was larger than in typical forests, and the data collecting flights in denser forests were manually piloted.

Therefore, open questions remain regarding the applicability and reliability of these algorithms in diverse forest environments, especially in challenging boreal forests.

### 3. Materials and methods

#### 3.1. *Autonomous navigation algorithms*

In this study, the objective was to develop a prototype lightweight camera-based drone capable of autonomously avoiding obstacles under the forest canopy and operating without GNSS. The drone was required to fly autonomously from the takeoff location to a specified goal point while recording stereo-camera data during the flight. This prototype will later serve as a development platform for more extended and sophisticated data collection tasks.

Among the open-source solutions presented in Section 2.2, the solution by Zhou et al. (2022) was chosen as the base of the prototype. The solution was the only open-sourced camera-based solution proven to work with only one stereo camera making it possible to build a smaller and lighter platform. Additionally, the test environment reported in the original article (dense bamboo forest) was the most difficult among the proposed solutions, even though it had a highly different structure than the typical boreal forests.

The main details of the algorithms used in the chosen solution are briefly described in the following, and the complete system architecture of the prototype is presented in Figure 1. For more detailed information, the readers are referred to the cited original sources.

##### 3.1.1. *EGO-Planner-v2*

The source code of the planner algorithm by Zhou et al. (2022) was named in Github as EGO-Planner-v2 (ZJU FAST Lab Team 2022a). Although EGO-Planner-v2 is designed for swarm flying, in this study, the algorithm was modified for a single drone system to focus on navigation performance in challenging forest environments. The planner runs on top of the Robot Operating System (ROS) (Quigley et al. 2009). The mapping of EGO-Planner-v2 is based on probabilistic occupancy grid maps (Moravec and Elfes 1985). The mapping module uses depth images as an input, and the system adopts the fixed-sized circular buffers proposed by Usenko et al. (2017) for maintaining the local map. The maps also have a virtual floor and a virtual ceiling defining the minimum and maximum altitudes of the grid map, respectively. The virtual floor and the virtual ceiling restrict the altitude at which the algorithm can plan the paths.

In the trajectory planning, EGO-Planner-v2 uses a MINCO (minimum control) (Wang et al. 2022) trajectory representation designed for differentially flat systems, such as quadrotors (Mellinger and Kumar 2011). Planned trajectories are represented as piece-wise polynomial splines with decoupled temporal and spatial parameters (Zhou et al. 2022). The trajectories are optimized iteratively by minimizing the weighted sum of metrics defined for trajectory smoothness and flying time. The feasibility of the planned trajectory is forced by deforming the shape to avoid obstacles and by restricting the magnitudes of trajectory velocity, acceleration, and jerk to fulfill the dynamical constraints of the drone. For computational efficiency, the trajectory constraints are enforced via integrals of penalty functions with large penalty weights, and the integrals are evaluated by a finite sum of equally spaced samples along the timeline. In a simplified

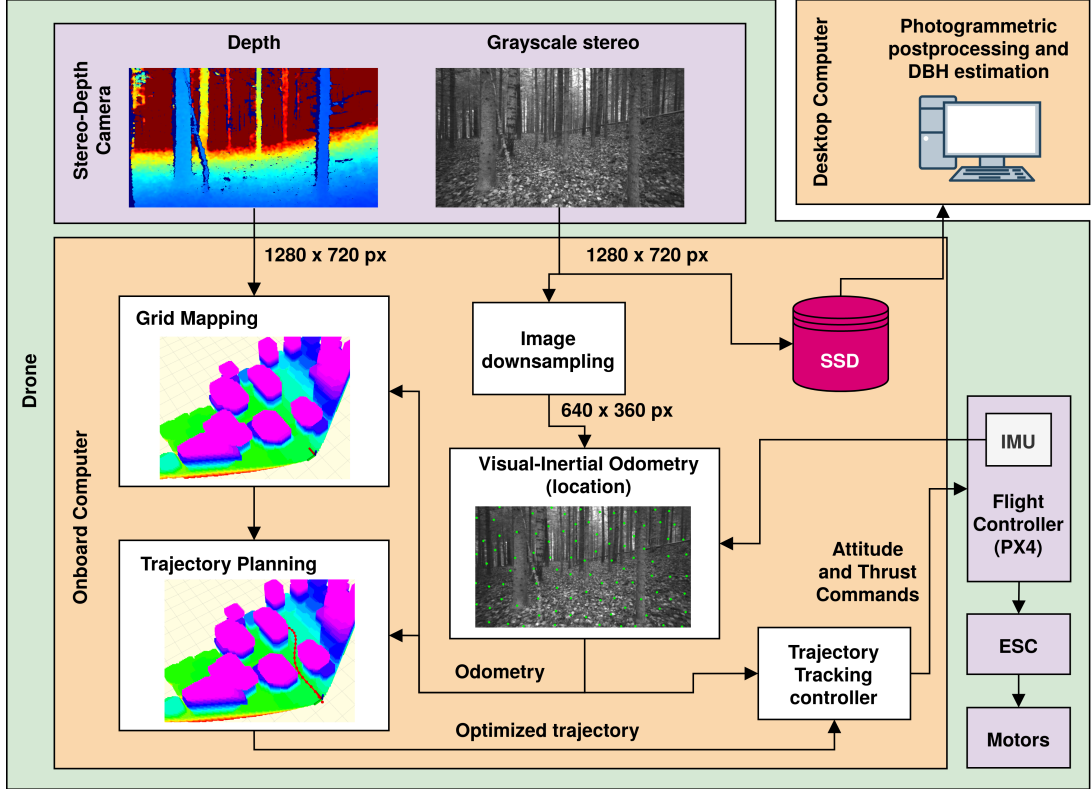


Figure 1.: The system architecture used in the data collection. In comparison to the original EGO-Planner-v2 article by Zhou et al. (2022), UWB-based Drift correction and Wireless trajectory broadcast network modules used for swarm navigation were omitted in this study. Stereo images were downsampled for VIO to guarantee real-time estimation. Full-resolution stereo images were also saved and post-processed to point clouds used in the DBH estimation.

form, the optimization of time-dependent objectives  $J$  in one piece of the trajectory can be represented by

$$\min \sum_x \lambda_x J_x \quad (1)$$

where  $J_x$  are the penalty terms and  $\lambda_x$  are the corresponding weights. Subscripts  $x = \{s, t, d, o, u\}$  stand for the trajectory smoothness, total flying time, dynamical feasibility, obstacle avoidance, and the uniform distribution of constraint evaluation points along the trajectory, respectively. In addition to the above-mentioned penalty terms, EGO-Planner-v2 also includes penalty terms for the swarm operations, but those are omitted here. A\* is utilized as the global path-search algorithm given as input for the optimization algorithm.

The trajectory planning is continuously performed within a defined local planning distance towards a user-defined global goal until the goal is reached. Since the safety constraints are modeled as integrals in the penalty functions, the feasibility of the trajectory needs to be verified with a post-check after planning (Zhou et al. 2022). Due to the non-static probabilistic map, the post-check after trajectory planning guarantees

feasibility only at a certain moment. Hence, a collision-check process is continuously running in the background. If that process detects a potential collision, a trajectory replanning is activated immediately. If the replanning fails and the predicted time to collision is under a given threshold, the planner performs an emergency stop. After the drone has stopped, the trajectory planner tries to start up again and find a new feasible trajectory.

### 3.1.2. VINS-Fusion

The Visual-inertial odometry (VIO) algorithm used by Zhou et al. (2022) was VINS-Fusion (Qin, Li, and Shen 2018; Qin et al. 2019b)(VINS stands for 'Visual-Inertial system'), which used grayscale stereo images and IMU data to track the position and orientation of the drone.

VINS-Fusion detects Shi-Tomasi corner features (Shi and Tomasi 1994), and the features are tracked between frames with Kanade-Lucas-Tomasi (KLT) Tracker (Lucas and Kanade 1981). IMU data is used for preintegration, i.e., position, velocity, and orientation are integrated from IMU measurements between two frames. The state optimization is performed within a sliding window, including the position, velocity, rotation, and IMU biases. To reduce the computational complexity, old measurements are marginalized into a prior of the estimation process. Certain frames are also selected as keyframes, which are saved to a global pose graph after being marginalized out from the sliding window. Keyframes are selected by considering the number of tracked features and the average parallax between these features in the most recent camera frame and the latest keyframe.

VINS-Fusion supports loop detection-based relocalization and global pose graph optimization to reduce the accumulated drift in the pose estimate. The loops are detected by storing additional corner features as BRIEF descriptors (Calonder et al. 2010) to DBoW2 (Galvez-López and Tardos 2012) bag-of-word database. After a loop detection, the relocalization process aligns the latest window to past poses and optimizes it utilizing also the feature correspondences with past poses. In addition to sliding window relocalization, the global pose graph is also optimized after loop detections to enforce the global consistency of the poses. Since the roll and pitch angle estimates are drift accumulation-free due to full observability from the gravity measurement of the IMU, the pose graph optimization is performed in 4 degrees of freedom.

VINS-Fusion also adopts an online temporal calibration method for inertial and visual measurements (Qin and Shen 2018). The method can be used to adjust the time offset  $t_d$  between the camera and the IMU online.

In the swarm operations of the original article (Zhou et al. 2022), the drones used also relative distances measured with Ultra Wide Band (UWB) sensors to correct the drift in the pose estimate of VINS-Fusion. However, with a single drone system in this study, that function is omitted.

The parameters used in the configuration of VINS-Fusion were chosen so that real-time performance was guaranteed. In the initial tests, the IMU noise values used during the calibration were over-optimistic for VINS-Fusion causing instability to the estimates, so the IMU noise values were increased more. All VINS-Fusion configuration parameters are listed in Table 2.

Table 2.: VINS-Fusion parameters.

Parameter	Value
Image resolution	$640 \times 360$
Max number of tracked features	150
Min distance between features	40 px
RANSAC threshold	1 px
Max solver iteration time	0.04 ms
Max solver iterations	8
Keyframe parallax threshold	10 px
Accelerometer noise SD	0.2
Gyroscope noise SD	0.05
Accelerometer random walk SD	0.002
Gyroscope random walk SD	0.0005

### 3.1.3. Tracking controller

The original EGO-Planner-v2 article (Zhou et al. 2022) did not specify the utilized method for trajectory tracking. In this study, an open-source tracking controller (ZJU FAST Lab Team 2022b) by Zhejiang University was used. The tracking controller gets setpoints for position, velocity, acceleration, and yaw from the trajectory planner and converts those to attitude and thrust setpoints. The setpoints are forwarded to the PX4 flight controller software (PX4 Community 2023) responsible for the low-level attitude and angular rate controls.

## 3.2. Drone hardware

In the physical robot drone prototype, an onboard computer NVIDIA Jetson Orin NX (Santa Clara, California, USA) was used. The used PX4-compliant autopilot was Holybro Kakute H7 (Hongkong, China), which also contained the IMU. The navigation algorithms mentioned in the previous subsection ran on top of the ROS, and the Mavros protocol was used for communication between the onboard computer and the autopilot. As a camera, Intel RealSense D435 (Intel Realsense Development Team 2023)(Keselman et al. 2017) was used. The camera was capturing both depth images for 3D mapping and grayscale stereo images for VIO.

RealSense D435 is based on active stereoscopy, and the camera has an infrared laser projector emitting dots that can be used for triangulation by the stereo camera. This can improve the triangulation in low-light conditions and to homogeneous surfaces that contain no features. However, the dots of the laser emitter cause problems for VIO since they are moving with the camera. In the previous set-up described by (Karjalainen et al. 2023), a modified version of the ROS-RealSense driver by Zhou et al. (2021b) was used. The modified driver turns the laser emitter of the camera constantly on and off, making it possible to produce high-quality depth images in every other frame and stereo images without the laser dots in every other frame. However, this solution comes with the drawback of halving the output frame rate of the camera.

In the first test flights described by (Karjalainen et al. 2023), difficulties were encountered in detecting small branches with a depth camera resolution of  $640 \times 480$ , leading to the decision to increase the depth camera resolution to a maximum value of

1280 × 720. The stereo images for VIO were downsampled at a resolution of 640 × 360 to ensure real-time performance. As the maximum frame rate of D435 at a resolution of 1280 × 720 is 30 Hz, the modified driver version would have resulted in a low frame rate of 15 Hz. To ensure the VIO performance in quick turns, the frame rate of 30 Hz was preferred, and hence, the IR emitter was disabled, making the camera function as a passive IR stereo camera. The choice can be further justified with the fact that the usefulness of the IR emitter in forest conditions is questionable since sunlight contains infrared light that can interfere with the emitted artificial features (Kuan, Ee, and Wei 2019), and the forests typically do not contain large homogeneous surfaces. The Realsense D435 onboard camera was configured to use the built-in automatic exposure control.

The camera-IMU system was calibrated with an open-source camera calibration toolbox, kalibr (Furgale, Barfoot, and Sibley 2012; Furgale, Rehder, and Siegwart 2013; Maye, Furgale, and Siegwart 2013). In the calibration, the intrinsic and extrinsic parameters of the left and right grayscale cameras and the time shift between the camera and the autopilot IMU were calculated from recorded data where Aprilgrid (Olson 2011) was used as a calibration target. The IMU noise parameters needed for the calibration were first obtained with the open source tool Allan Variance ROS (Oxford Dynamic Robot Systems Group 2022), and the values obtained were multiplied by 10 before the calibration as suggested in the wiki of the kalibr project (ETH Zürich Autonomous Systems Lab 2023).

The computer, the camera, and the autopilot were attached to a 330 mm drone frame. The propellers had two pieces of 6 cm long blades each. The measured weight of the drone, including the motors and the onboard computer, was 791 g without batteries and 1153 g with the batteries. An overview of drone hardware is presented in Figure 2.



Figure 2.: The drone hardware used in the flight tests with a forward-facing Realsense D435 camera. Nvidia Jetson Orin NX onboard computer is hidden in the case under the drone frame. Holybro Kakute H7 Flight controller unit is located inside the frame. Batteries (not visible in the picture) are mounted on the top of the drone frame.

### 3.3. Test sites

The performance of the system was evaluated in three different boreal forest areas. The flight tests of the system were performed in two test areas located in Evo, Finland (61.19°N, 25.11°E). The flight paths went through well-documented forest sample plots that have been widely used in previous studies, such as in Liang et al. (2018, 2019); Wang et al. (2019); Hyypä et al. (2020a,c), and are classified into three complexity categories, i.e., 'easy', 'medium', and 'difficult' based on, mainly tree density and amount of vegetation under the canopy in the plots. The third test area, a spruce forest in Paloheinä, Finland (60.26°N, 24.92°E) was used only to test the loop detection performance of VINS-Fusion.

The first plot in Evo has been classified as 'medium' (Figure 3), and the second has been classified as 'difficult' (Figure 4). The medium-difficulty plot had a tree density of 650 trees/ha and a mean DBH of 28 cm. The most common tree species in the plot were Norway spruce (*Picea abies* (L.) H.Karst.)(81.2 %) and Scots pine (*Pinus sylvestris* L.)(9.4 %). The difficult forest had a tree density of 2000 trees/ha and a mean DBH of 17 cm. The most common tree species in the plot were Norway spruce (64.4 %) and aspen (*Populus tremula*, L.) (18.3 %). Only trees with a DBH greater than 5 cm were included in these statistics. From now on, these two test areas are called 'Evo-medium' and 'Evo-difficult', respectively.



Figure 3.: View from the first takeoff location in the 'Evo-medium' test area. The takeoff location was changed after five test flights.

For reference purposes, circular GCPs provided by Agisoft Metashape (Agisoft LLC, St. Petersburg, Russia) were placed within the forest plots used in the flight tests. The



Figure 4.: View from the takeoff location in the 'Evo-difficult' test forest.

targets had a diameter of 24.7 cm and the middle dots had a size of 7 cm. Relative distances between the GCPs were measured with Leica Nova TS60 total station with a precision of approximately 2 mm (Leica Geosystems 2020). Figure 5 shows GCPs in 'Evo-difficult' during the test flights.

GCPs were not used in the third test forest, 'Paloheinä'. The experiment there aimed to test the loop detection performance of VINS-Fusion in a homogeneous forest environment without any artificial targets. The data were collected by walking with the drone. The estimated average tree density in the area was approximately 2000 trees/ha.

### 3.4. *Flight tests*

Test flights in Evo were conducted on 18th October 2023. Multiple test flights were performed to evaluate the forest-type effects on the performance of autonomous navigation. In total, seven test flights were conducted in the 'Evo-medium' test area and nine test flights in the 'Evo-difficult' test area. In each test environment, either the takeoff location or the takeoff heading was altered during the test flight campaign to force the drone to follow different paths. In the 'Evo-medium' test area, the takeoff location was changed after five test flights. In the 'Evo-difficult' test area, the takeoff heading was changed after six test flights. The target flight velocity was 1 m/s in all flight tests. The goal was set 36 m forward in the first takeoff location in the 'Evo-medium' test area, 34 m forward in the second takeoff location in the 'Evo-medium' test area, and 42 m forward in the takeoff location in the 'Evo-difficult' test area. The maximum flight



Figure 5.: GCPs for reference trajectory generation in 'Evo-difficult' forest. Targets were spread widely to the test site to increase the probability that there would be targets visible in the recorded camera data regardless the path that the robot takes.

height was set to 2.25 m relative to the takeoff location in the 'Evo-medium' test area. For the first test flight in the 'Evo-difficult' test area, the maximum flight height was set to 2.5 m with respect to the takeoff location and was increased to 2.75 m for the rest of the flights.

The campaign to evaluate the loop detection capability took place on 26th January 2024. Stereo images and IMU data were collected during two walks inside the forest while carrying the drone by hand. The paths of the walks were approximately 340 m and 240 m long, each containing multiple loops where the same scene was observed multiple times. The data collection took place during winter, with the forest covered in snow.

### ***3.5. Structure-from-Motion Multi-View Stereo based reconstruction***

Photogrammetric Structure-from-Motion Multi-View Stereo (SfM-MVS) processing was conducted in post-processing mode to generate 3D point clouds for DBH estimation and to generate reference trajectories for evaluating VIO performance.

Stereo image processing was carried out using Agisoft Metashape software (Agisoft LLC, St. Petersburg, Russia) (Metashape Development Team 2021) following similar processing steps as introduced by Viljanen et al. (2018). Every sixth stereo pair was used in the Metashape processing with a stereo baseline of 5 cm and an accuracy

setting of  $\pm 0.0015$  m. In the image orientation processing, the quality setting was set to high meaning that two times downsampled images were used. The settings for the number of key points and tie points per image were 40,000 and 4,000, respectively. To enhance the quality of the post-processed reference trajectories, GCPs were used in the processing with an accuracy setting of  $\pm 0.005$  m. Automatic outlier removal was performed using gradual selection tools of the software based on re-projection error, reconstruction uncertainty, and projection accuracy. Subsequently, a bundle adjustment was carried out, involving optimization of the sparse point cloud along with the interior (IOP) and the exterior orientation parameters (EOP). Following that, a dense point cloud was calculated using the highest quality setting and mild depth filtering. Finally, the EOPs and dense point clouds were exported.

Point clouds for DBH estimation were derived using datasets from four flights conducted in the 'Evo-medium' test area, each designated as follows: I: the first flight, II: the second flight, III: the third flight, IV: the fourth flight, and I-IV: combined processing of all four flights (Combined). The processing was carried out using all GCPs. Additionally, to evaluate the impacts of GCPs, point clouds were generated from the first flight trajectory processed with different GCP configurations, denoted as:  $I_{0GCP}$ : no GCPs,  $I_{1GCP}$ : one GCP at the beginning of the trajectory,  $I_{2GCP}$ : two GCPs, one at the beginning and one at the end of the trajectory, and  $I_{3GCP}$ : three GCPs, positioned at the beginning, middle, and end of the trajectory.

The experiments were conducted in dense forests, where collecting reference data using GNSS was not possible due to the forest canopy blocking the signal. Reference trajectories were generated for the flights using SfM processing. In each case, the reference trajectory was derived from the first takeoff heading and orientation in both Evo test environments. Figure 6 visualizes the GCPs, stereo images, and reference trees during the point cloud processing in the Agisoft Metashape.

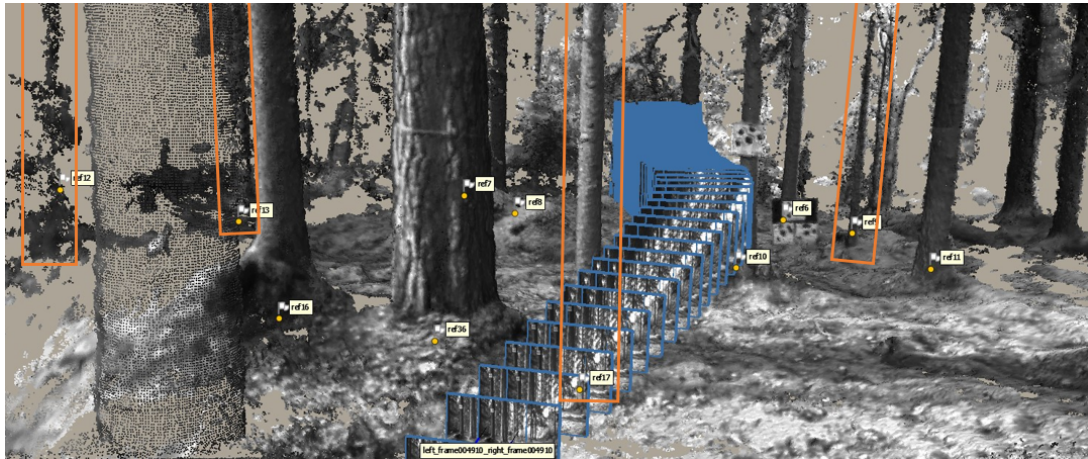


Figure 6.: GCPs, stereo images and reference trees visualized during the point cloud processing in the Agisoft Metashape (Metashape Development Team, 2021). Detected reference trees are marked, while those not detected are highlighted with a orange box.

### 3.6. *Tree parameter estimation*

In this study, trees were detected, and their DBHs were estimated using an automatic stem diameter estimation algorithm proposed by Hyyppä et al. (2020b) and further developed by Hyyppä et al. (2020a) to be suitable for a larger variety of point clouds, including photogrammetric point clouds, and point clouds produced with 3D mobile laser scanners and TLS. The method described by Hyyppä et al. (2020a) was applied to estimate the DBH from point clouds collected with the drone and a TLS system, the latter of which provided reference measurements of DBH (see details in Section 3.7).

The point cloud was first segmented into 40-cm-tall (20-cm-tall for TLS) vertical segments, and 5-s-long temporal segments. The temporal segmentation was done to mitigate point cloud distortions caused by potential slowly-accumulating positioning errors of the moving drone system, and thus, the temporal segmentation was not performed for the TLS data. The points potentially corresponding to the tree stems were detected by clustering the points with density-based clustering (DBSCAN, (Ester et al. 1996)) and filtered by fitting a circle to each cluster while accepting only those clusters satisfying the following heuristic criteria: the cluster contained more than 35 points and at least 80 % of the points within 30 mm of the circular arc, the fitted circle radius was between 4 cm and 40 cm, and the points covered at least a 60° central angle of the fitted circle. The accepted clusters were further grouped into tree stems by applying DBSCAN for the center points of the clusters, and the growth direction of each tree was estimated with principal component analysis (PCA). The points within accepted clusters were projected into the plane perpendicular to the growth direction for the final diameter estimation. The diameters were processed into a stem curve by automatically removing clear outliers, followed by fitting a smoothing spline to the remaining diameter estimates as a function of height. Finally, the DBH estimates were calculated by interpolating the stem curve at the height of 1.3 m above the ground. For a detailed description of the method, the reader is referred to Hyyppä et al. (2020b,a).

### 3.7. *Performance assessment*

#### 3.7.1. *Autonomous flying performance*

The performance and reliability of the autonomous flight of the prototype were evaluated based on two factors: the reliability of the obstacle avoidance and the accuracy of the VIO localization.

Obstacle avoidance reliability was evaluated based on the mission success. A mission was considered successful if the drone reached the end of the flight without major collisions. Minor touches to thin vegetation or branches were allowed if the drone was able to continue the mission after that. If the given goal was inside an obstacle, the mission was considered successful if the drone managed to fly next to the goal. In addition to obstacle avoidance, the smoothness of the trajectory was assessed. The trajectory was considered smooth if the system did not perform any emergency stops during the flight.

The accuracy of the VIO localization was evaluated by calculating the Absolute Trajectory Error (ATE), as proposed by Sturm et al. (2012), with respect to the post-processed SfM reference trajectories. In this study, ATE was calculated only for the position estimate, and the error in the orientation estimate was not evaluated. ATE was calculated using the trajectory evaluation toolbox by Zhang and Scaramuzza (2018), which aligns the trajectory estimates with the reference trajectories with the method

by Umeyama (1991). After aligning the trajectories, the toolbox calculates the RMSE of the individual state errors to generate a single metric error value representing the accuracy of the entire trajectory. In the mathematical form, the error can be presented as

$$\text{ATE}_{\text{pos}} = \left( \frac{1}{N} \sum_{i=0}^{N-1} \|\Delta \mathbf{p}_i\|^2 \right)^{\frac{1}{2}} \quad (2)$$

where  $\Delta \mathbf{p}_i$  is the error between the estimated position and reference trajectory position in a single state.

In the first tests conducted in a simulator as described by (Karjalainen et al. 2023), the VINS-Fusion estimate was found to be more accurate when the  $t_d$  value was fixed to constant, compared to when the online estimation method (Qin and Shen 2018) was used. For this reason, during the test flights, the  $t_d$  value was fixed to the one obtained from kalibr. However, the calibration estimate is never perfect, and the prototype did not have actual hardware synchronization between the camera and the autopilot IMU. For that reason, after the test flights, the VINS-Fusion estimation was also run with online estimated  $t_d$  with the camera and IMU data recorded during the flight tests. The estimates were performed with the onboard computer of the drone, and the  $t_d$  estimate obtained with kalibr was used as the initial value of online estimation.

The loop detection capability of VINS-Fusion was evaluated in a natural forest environment in Paloheinä, without the use of artificial targets that could affect the system performance. Since there were no GCPs for forming the reference trajectories, only the ability to detect the loops inside dense natural forests was tested, and the accuracy of the loop-corrected trajectory was not evaluated. VINS-Fusion estimate with the loop detection algorithm was run for the collected data with the onboard computer of the drone, and the effect of a maximum number of features in pictures for loop detection capability was examined.

### 3.7.2. DBH estimation performance

The accuracy of the DBH estimation from the drone point cloud data was evaluated using TLS data as a reference. The TLS scannings were conducted in April 2020, and tree height, DBH, and other parameters were estimated from the dataset. The estimated error of the DBH measurement was less than 1 cm.

Several metrics were used to evaluate the accuracy of the DBH estimation, including RMSE, Relative RMSE (RMSE %), Bias, Relative Bias (bias %), and Standard Deviation.

The RMSE measures the square root of the average of the squared differences between the estimated and reference DBH values. Bias indicates the average deviation between the estimated and reference DBH values.

$$\text{RMSE} = \sqrt{\frac{1}{n} \sum_{i=1}^n (d_{\text{estimated},i} - d_{\text{reference},i})^2} \quad (3)$$

where  $n$  is the total number of observations,  $d_{\text{estimated},i}$  is the estimated DBH, and  $d_{\text{reference},i}$  is the reference DBH.

$$\text{Bias} = \frac{1}{n} \sum_{i=1}^n (d_{\text{estimated},i} - d_{\text{reference},i}) \quad (4)$$

Relative RMSE (RMSE %) is computed by dividing the RMSE by the mean of the reference DBH values and multiplying by 100 to express it as a percentage. Relative Bias (Bias %) is determined by dividing the Bias by the mean of the reference DBH values and multiplying by 100.

$$\text{Relative RMSE (\%)} = \frac{\sqrt{\frac{1}{n} \sum_{i=1}^n (d_{\text{estimated},i} - d_{\text{reference},i})^2}}{\bar{d}_{\text{reference}}} \times 100 \quad (5)$$

$$\text{Relative Bias (\%)} = \frac{\frac{1}{n} \sum_{i=1}^n (d_{\text{estimated},i} - d_{\text{reference},i})}{\bar{d}_{\text{reference}}} \times 100 \quad (6)$$

Additionally standard deviation was calculated with following equation:

$$\text{SD} = \sqrt{\frac{1}{n} \sum_{i=1}^n (d_{\text{estimated},i} - \bar{d}_{\text{reference}})^2} \quad (7)$$

where  $\bar{d}_{\text{reference}}$  is the mean of the reference DBH values, and SD is the standard deviation.

The completeness of stem detection was evaluated by comparing the total number of reference trees found from the drone-collected point cloud data to the total number of reference trees within the point cloud boundary.

$$c = \frac{r}{t} \times 100 \quad (8)$$

where  $c$  represents completeness (%),  $r$  is the number of reference trees found, and  $t$  is the total number of reference trees.

The impact of tree growth between the collection of drone data and reference measurements (four growth seasons) was not taken into account. Variability in tree growth, influenced by factors such as species, locations, health, and age, is acknowledged as a source of error. Considering that the tree growth was relatively constant in the test area, forming a major component of the bias in the estimates. Additionally, some reference trees fell between the measurements and were not included in the estimations.

## 4. Results

### 4.1. *Autonomous navigation performance*

#### 4.1.1. *Obstacle avoidance*

The task of avoiding collisions during the flight is naturally more demanding in a dense forest than in a sparse forest. Consistent with these expectations, the trajectories were

smoother and the success rate was better in 'Evo-medium' than in 'Evo-difficult' test area. In 'Evo-medium', all performed test flights were successful and five out of seven test flights were performed with smooth trajectories without any emergency stops during the flight. In 'Evo-difficult', one of nine test flights failed. None of the test flights in 'Evo-difficult' was performed with a smooth trajectory. However, despite the emergency stops during the flight, the system was still able to continue the mission after the stops, leading to a successful mission in eight of the nine test flights.

The reason for emergency stops in both environments was the late detection of thin and dry spruce branches. In the failed test flight in 'Evo-difficult' the reason was also a collision to a similar thin low branch.

The test flight success rates in both test forests are summarized in Table 3. Figure 7 presents examples of performed trajectories and obtained point clouds in both test forests.

Table 3.: Test flight success in the test forests

Test areas	Forest type	Density (trees/ha)	Flight lengths (m)	Successful flights	Smooth trajectories
'Evo-medium'	Old Spruce forest	650	34 - 36	7/7	5/7
'Evo-difficult'	Young Spruce forest	2000	42	8/9	0/8

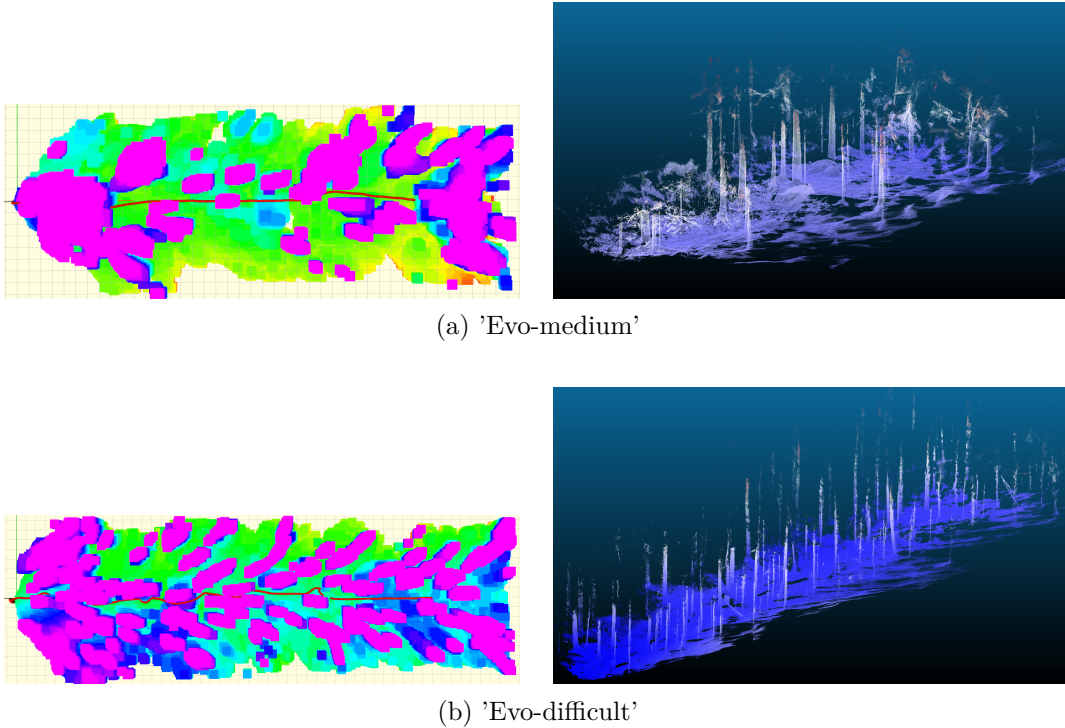
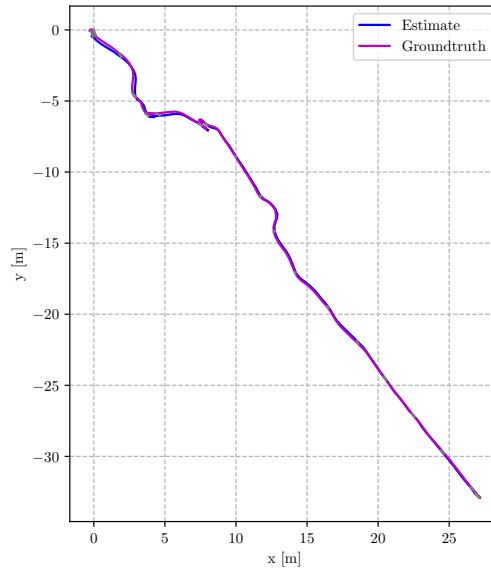


Figure 7.: Examples of drones' own navigation grid maps with performed trajectories (left) and obtained point clouds (right) in (a) 'Evo-medium' and (b) 'Evo-difficult'

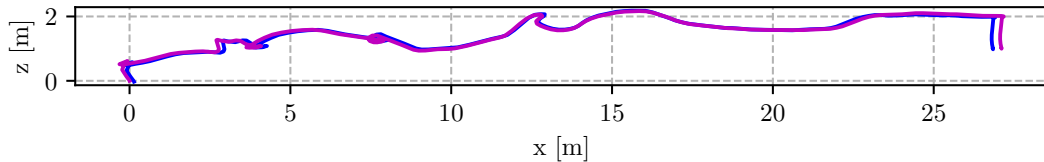
#### 4.1.2. VIO

The trajectory estimate error against the reference trajectory was calculated for the first five flights in 'Evo-medium' and for three flights in the difficult forest. The flights from the second takeoff location in 'Evo-medium' and from the second takeoff orientation in 'Evo-difficult' were not used in the VIO estimation since GCPs used in the reference trajectory processing were positioned along the first flight trajectories in both environments. In 'Evo-difficult', one of the flights from the first takeoff orientation was performed without GCPs, leading to a non-comparable reference trajectory, one of the flights had a data recording error during a flight, and in one flight, Metashape failed to retrieve the reference path.

Figure 8 shows an example of the VINS-Fusion trajectory estimate compared to the reference in 'Evo-difficult' while Table 4 summarizes the VINS-Fusion estimation errors across all flights. The average  $ATE_{\text{pos}}$  was 0.50 m in 'Evo-medium' and 0.34 m in 'Evo-difficult' with standard deviations of 0.06 m and 0.07 m, respectively, without online  $t_d$  estimation. The VINS-Fusion estimates with online  $t_d$  estimation were computed post-flight for the same trajectories, yielding an average  $ATE_{\text{pos}}$  of 0.47 m in 'Evo-medium' and 0.33 m in 'Evo-difficult' with standard deviations of 0.02 m and 0.04 m, respectively.



(a) Top view.



(b) Side view.

Figure 8.: Example of a VINS-Fusion trajectory estimate and a reference trajectory obtained with Agisoft Metashape in the 'Evo-difficult' forest from a) top and b) side.

Table 4.: VINS-Fusion estimation Errors in all test flights

Test area	Flight No.	$ATE_{\text{pos}}$ (constant $t_d$ )	$ATE_{\text{pos}}$ (online estimated $t_d$ )
'Evo-medium'	1	0.5567	0.4816
'Evo-medium'	2	0.5599	0.4790
'Evo-medium'	3	0.4538	0.4769
'Evo-medium'	4	0.4945	0.4722
'Evo-medium'	5	0.4313	0.4400
'Evo-difficult'	1	0.3787	0.3340
'Evo-difficult'	2	0.3853	0.3727
'Evo-difficult'	3	0.2680	0.2962

The small standard deviations between the  $ATE_{\text{pos}}$  estimates indicated that the error between the VINS-Fusion trajectories and the reference trajectories was similar across all flights. In each case, VINS-Fusion accurately captured the trajectory shape but systematically underestimated the total flight distance.

Figure 9 shows an example of a VINS-Fusion tracking image during a test flight in 'Evo-difficult'. The algorithm detects stable features to track from all parts of the picture. The image also shows flying dry leaves blown up by the airflow from the propellers of the drone. The moving leaves did not cause visible disturbances to the tracking of the pose.

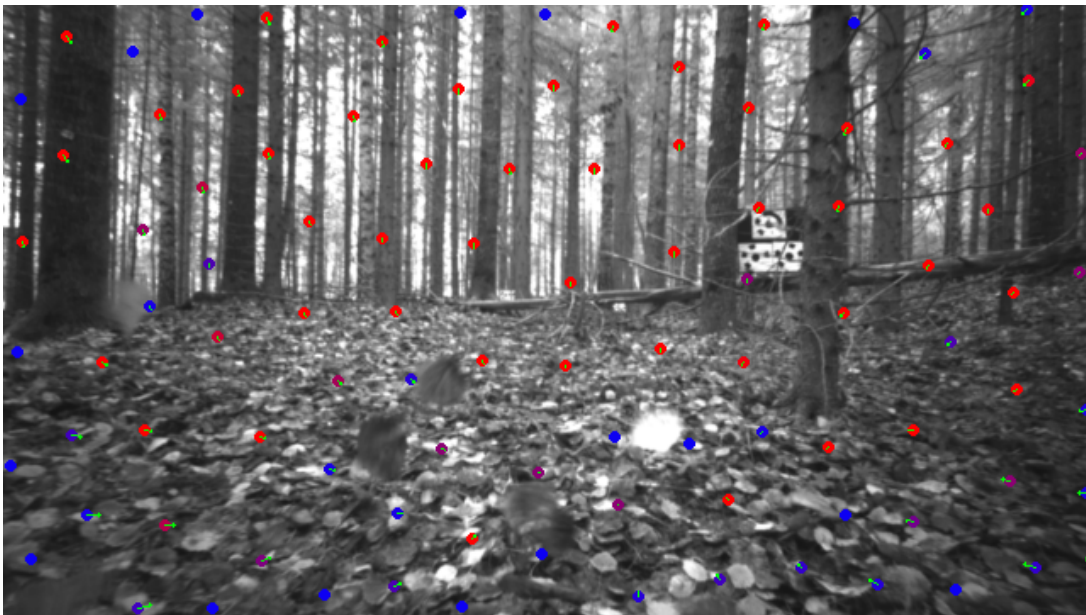
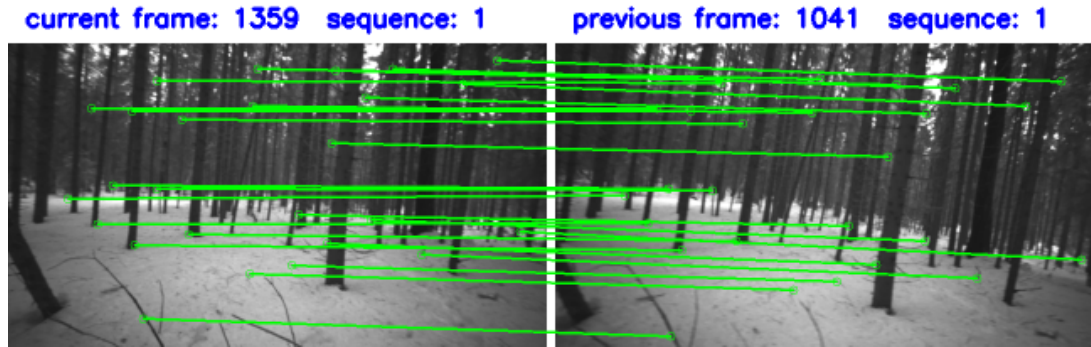


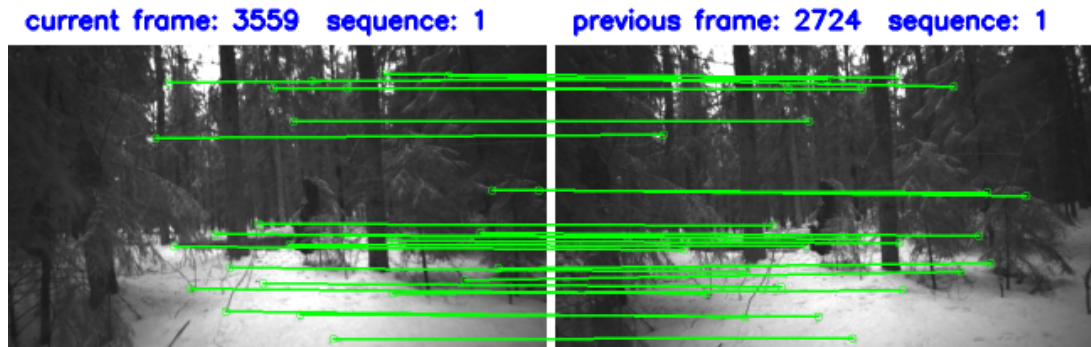
Figure 9.: Example of VINS-Fusion tracking image visualizing the tracked features. The tracking was not disturbed by the dry leaves blown by the air flow from the propellers of the drone. The coloring of the feature markers depends on the time how long the feature has been tracked. Blue dots symbolize new features and red features have been tracked longer.

In the loop closure tests, VINS-fusion detected a loop closure between 20 image pairs in the shorter path and four image pairs in the longer path with the same feature tracking

parameters (Table 2) that were used in the flight tests. Figure 10 shows examples of detected loop closure image pairs from both paths. The number of detected loops can be increased by increasing the number of features per image in the VINS-Fusion configuration. By reducing the minimum distance between features from 40 to 35 pixels, VINS-Fusion detected a loop closure between 52 image pairs in the shorter path and 23 image pairs in the longer path. By decreasing the minimum distance between features to 30 pixels, VINS-Fusion detected a loop closure between 82 image pairs in the shorter path and 63 image pairs in the longer path. However, increasing the number of features also increases the computational burden of the VIO, and the effects on the real-time performance during flying were not tested in this study.



(a) Shorter path.



(b) Longer path.

Figure 10.: Example of image pairs where VINS-Fusion detects a scene to already visited one and performs a loop closure.

## 4.2. Forest reconstruction and analysis

### 4.2.1. Photogrammetric processing

Results of the photogrammetric processing are given in Table 5. In the image alignment process, all images were aligned in each dataset, which indicated successful processing. Re-projection errors varied between 0.29 and 0.39 pixels. The estimated GSDs (Ground Sampling Distance) ranged between 4.08 and 6.17 mm at ground level. Distances from the trees varied between 0.55 and 7.94 m, resulting in GSDs of 0.85-12.34 mm at the ob-

jects of interest. Point clouds from datasets II-IV had similar point densities of 2.63-2.84 points/cm<sup>2</sup>, while dataset I provided a slightly higher point density of 3.58 points/cm<sup>2</sup>.

Table 5.: Photogrammetric processing results. Img. count: Number images/Number of aligned images; Number of GCPs; Completeness % (Number of trees found/Number of total trees); Reprojection error (pix); Number of tie points (in millions); Point density (points/cm<sup>2</sup>) in 'Evo-medium' test site. I: Trajectory 1, II: Trajectory 2, III: Trajectory 3, IV: Trajectory 4, Combined: Trajectories 1-4 merged, and for Trajectory 1  $I_{0GCP}$ : no GCPs,  $I_{1GCP}$ : 1 GCP,  $I_{2GCP}$ : 2 GCPs,  $I_{3GCP}$ : 3 GCPs

Dataset	Img. count	N GCPs	Completeness (%)	Reproj. error (pix)	Num. tie points (millions)	Point density (points/cm <sup>2</sup> )
I	650/650	15	79.31 (23/29)	0.39	197132	3.58
II	648/648	15	62.07 (18/29)	0.33	151889	2.84
III	619/619	11	61.29 (19/31)	0.33	151083	2.63
IV	597/597	15	62.50 (20/32)	0.33	141716	2.66
Combined	2514/2514	15	33.33 (12/36)	0.29	1547828	8.53
$I_{0GCP}$	650/650	0	72.41 (21/29)	0.39	197132	3.54
$I_{1GCP}$	650/650	1	68.97 (20/29)	0.39	197132	3.54
$I_{2GCP}$	650/650	2	75.86 (22/29)	0.39	197132	3.54
$I_{3GCP}$	650/650	3	79.31 (23/29)	0.39	197132	3.54

Results of accuracy estimation using Check Points (CPs) are shown in Table 6. The cases without GCPs or with one GCP at the beginning of the trajectory provided similar 2D and 3D RMSEs of 11.36-11.72 cm and 11.37-11.73 cm, respectively. When two GCPs were used, the 2D and 3D RMSEs improved to 5.26 cm and 5.48 cm, respectively. Adding an additional GCP resulted in a significant improvement in the 2D and 3D RMSE, reducing them to 1.41 cm and 1.48 cm, respectively.

Table 6.: Accuracy estimation (RMSE) using Check Points (CPs) and Camera Location in 'Evo-medium' test site, for trajectory 1:  $I_{0GCP}$ : no GCPs,  $I_{1GCP}$ : 1 GCP,  $I_{2GCP}$ : 2 GCPs,  $I_{3GCP}$ : 3 GCPs

Dataset	Check Points (CPs) RMSE (cm)						Camera location RMSE (cm)				
	N CPs	X	Y	Z	2D	3D	X <sub>0</sub>	Y <sub>0</sub>	Z <sub>0</sub>	2D <sub>0</sub>	3D <sub>0</sub>
$I_{0GCP}$	15	6.99	8.95	0.65	11.36	11.37	7.06	9.07	0.30	11.49	11.50
$I_{1GCP}$	14	7.19	9.25	0.56	11.72	11.73	7.03	9.06	0.28	11.47	11.47
$I_{2GCP}$	13	5.01	1.61	1.52	5.26	5.48	7.03	9.06	0.28	11.47	11.47
$I_{3GCP}$	12	1.19	0.75	0.45	1.41	1.48	1.46	0.70	0.56	1.62	1.71

#### 4.2.2. Tree detection

Figure 11 shows post-processed trajectories for dataset I-IV, as well as reference and detected trees and the boundaries of the point clouds. I and II followed almost the same trajectory, while III and IV had similar trajectories. Dataset I trajectory was the smoothest, and it did not include any sharp turns. The other three trajectories had one or more sharper turns. For datasets I, II, III, and IV, the number of reference trees inside the point cloud boundary was 29, 29, 31, and 32, of which 23, 18, 19, and 20 were found from the drone-collected point clouds, respectively. The resulting completeness values were 79.31 %, 62.07 %, 61.29 % and 62.5 %, respectively. The total number of different trees found was 29 out of 33 (87,88 %) from dataset I-IV. However, when all the flights were processed simultaneously (combined) that resulted in only 33.33 % completeness, where only 12 of 36 trees were found. When utilizing 0, 1, 2, and 3 GCPs in the dataset

I, completeness values were 72.41 %, 68.97 %, 75.86 %, and 79.31 %, respectively (Table 5).

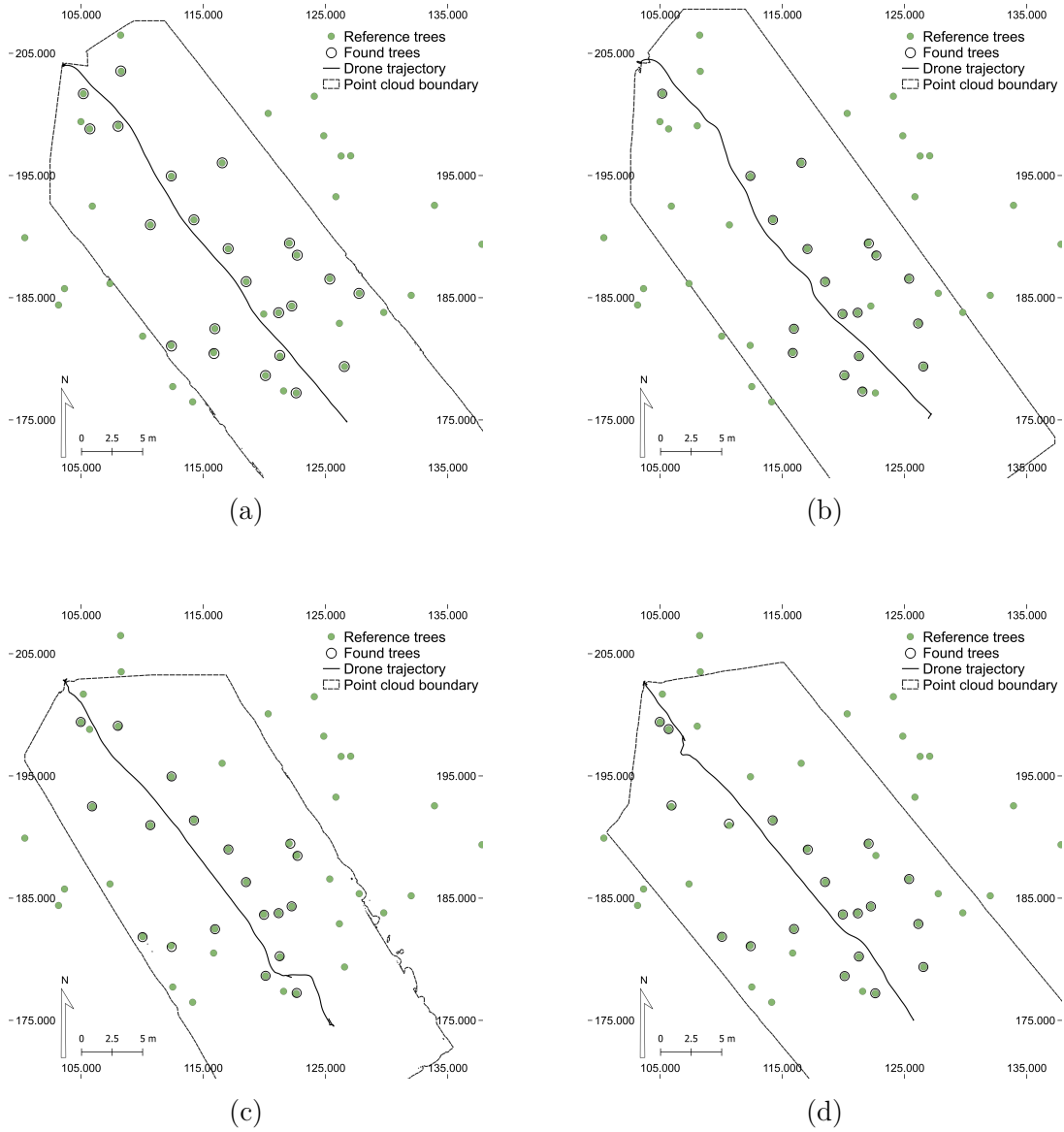


Figure 11.: Post-processed trajectories, reference trees and found trees in Dataset (a) I (b) II (c) III (d) IV

In dataset I, the stem detection algorithm failed to detect one large tree and two small trees located near the flight trajectory despite these trees being well-reconstructed in the point cloud. Similarly, the number of well-reconstructed trees but not detected by the algorithm was 4, 5, and 5, in datasets II, III, and IV, respectively. The three extra trees that were not identified in dataset I were situated further from the trajectory and exhibited poor reconstruction quality in the point cloud. The datasets II through IV each contained seven poorly reconstructed trees. Many of these trees were located at a greater distance from the trajectory, while others were obscured from the view of the camera by intervening trees.

### 4.2.3. DBH estimation

RMSE and bias of the DBH estimates of datasets I-IV were similar, ranging from 3.33 to 3.86 cm (10.69 %-12.98 %) and -0.67 to 1.40 (-2.11 %-4.71 %), respectively (Table 7). Processing four flights simultaneously (Combined) provided only marginally better results with an RMSE of 2.91 cm (9.14 %) and a bias of 1.51 cm (4.74 %).

When considering the impact of the number of GCPs, the utilization of 3, 2, 1, and 0 GCPs in photogrammetric processing yielded slightly poorer results compared to those obtained with all GCPs. The RMSE and bias values ranged from 3.93 to 4.37 cm (13.68 %-14.66 %) and 1.12 to 2.13 cm (3.89 %-7.55 %), respectively (Table 7).

Tree size had an impact on the DBH estimation accuracy (Table 7). For small and medium-sized trees with a DBH smaller than 30 cm, DBH estimations achieved superior performance in all datasets, with RMSE and bias varying from 1.16 to 2.75 cm (5.74 %-12.47 %) and -0.01 to 0.62 cm (-0.06 %-3.14 %), respectively. Significantly poorer performance was obtained for trees with a DBH greater than 30 cm, with RMSE and bias ranging from 4.04 to 11.08 cm (8.99 %-25.44 %) and -0.66 to 2.08 cm (-1.53 %-5.65 %), respectively.

Analysis of the impact of the camera distance from trees did not reveal a significant correlation between tree distance and DBH estimation errors.

Table 7.: Accuracy of the stem diameter breast height (DBH) in 'Evo-medium' test site. Dataset is split in 3 categories: All, DBH < 30 cm and DBH > 30 cm trees. Datasets: I: Flight 1, II: Flight 2, III: Flight 3, IV: Flight 4, Combined: Flights I-IV merged, and for Dataset I:  $I_{0GCP}$ : with no GCPs,  $I_{1GCP}$ : with 1 GCP,  $I_{2GCP}$ : with 2 GCPs,  $I_{3GCP}$  with 3 GCPs.

Dataset	Number of trees	RMSE (cm)		RMSE %		Bias (cm)		Bias %		Standard Deviation
		All	All	All	All	All	All	All	All	
		<30 cm	>30 cm	<30 cm	>30 cm	<30 cm	>30 cm	<30 cm	>30 cm	>30 cm
I	23	3.86	12.98	1.40	4.71	3.60				
	14	2.56	12.47	0.17	0.85	2.54				
	9	5.29	11.98	1.23	2.78	4.26				
II	17	3.33	12.79	1.01	3.87	3.17				
	12	2.16	11.36	0.31	1.63	2.12				
	5	5.14	12.01	0.70	1.63	4.56				
III	19	3.97	12.05	0.97	2.95	3.85				
	9	1.16	5.74	0.13	0.64	1.13				
	10	5.36	12.07	0.84	1.89	5.12				
IV	20	3.40	10.69	-0.67	-2.11	3.33				
	10	1.28	6.21	-0.01	-0.06	1.28				
	10	4.63	10.77	-0.66	-1.53	4.44				
Combined	12	2.91	9.14	1.51	4.74	2.49				
	7	1.41	6.70	-0.12	-0.56	1.39				
	6	4.04	8.99	1.63	3.62	1.87				
$I_{0GCP}$	21	4.37	14.66	1.61	5.42	4.06				
	12	2.75	13.07	-0.20	-0.97	2.73				
	9	7.93	18.62	2.41	5.65	5.17				
$I_{1GCP}$	20	4.38	14.71	1.68	5.65	4.04				
	12	2.02	9.63	-0.01	-0.06	2.02				
	8	6.46	15.06	1.69	3.95	4.88				
$I_{2GCP}$	23	4.35	15.43	2.13	7.55	3.79				
	14	1.77	8.98	0.62	3.14	1.48				
	8	11.08	25.44	2.08	4.77	8.96				
$I_{3GCP}$	23	3.93	13.68	1.12	3.89	3.77				
	14	1.22	6.23	0.14	0.72	1.20				
	9	6.10	14.20	0.98	2.27	5.57				

## 5. Discussion and Conclusions

### 5.1. *Autonomous flying*

The performance of autonomous navigation was promising in both test forests. The obstacle avoidance success rate was 100 % in the 'Evo-medium' forest and 87.5 % in the 'Evo-difficult' forest. However, the smoothness of the trajectories suffered from the increasing forest density. While in 'Evo-medium' 71.4 % of the flights had a smooth trajectory, in 'Evo-difficult' at least one emergency stop was needed in all of the flights. However, apart from the one failed flight in 'Evo-difficult', the system was able to do a successful trajectory re-planning and finish the mission after the emergency stops. Further consideration should be given to finding the optimal sensor for detecting thin and dry branches earlier. Nonetheless, the current prototype already allows reliable and safe autonomous obstacle avoidance in easy and medium-difficulty level boreal forests.

The accuracy of the position estimate by VINS-Fusion was satisfying for short flights performed in this study, but in the longer flights, the error would start to accumulate, making the position errors high. However, the standard deviation between the errors between the test flights was small, and the VINS-Fusion systematically estimated the flight paths shorter than in reality (as can be seen from Figure 8). This indicates that a notable part of the position error could be eliminated by improving the system calibration. The results indicate that the estimates by VINS-Fusion were more accurate with online  $t_d$  estimation than when the  $t_d$  value was fixed to the one obtained from the calibration. However, further development of the prototype should include implementing hardware-level synchronization between the camera and the IMU of the autopilot.

The position error can also be reduced by optimizing the estimate with loop closures, and the results from the walking tests show that VINS-Fusion could detect loop closures even in a homogeneous forest environment. Increasing the number of features tracked by VINS-Fusion increased the number of detected loops. However, increasing the number of features also increases the computational burden of the system, potentially disrupting the real-time estimation. Finding the optimal value for the tracked features, as well as measuring the actual improvement of the loop closures to the position estimate, requires further studies.

### 5.2. *Accuracy of forest measurements*

The proposed system was assessed by comparing it to other relevant studies (Section 2.1, Table 1) considering the accuracy, system autonomy, weight, and complexity of the test environment.

The RMSEs reported in the relevant studies varied from 3.2 % to 61.41 %. The highest accuracy UAV SfM-MVS results were presented by Shimabuku, Konoshima, and Ota (2023) with RMSEs of 0.4 cm (3.2 %) and 0.7 cm (3.6 %) in two test forest sites. However, their test sites included only 7 and 18 reference trees, and the semi-autonomous commercial drone system needed manual control to avoid horizontal obstacles. Kuželka and Surovỳ (2018), He et al. (2025), and Krisanski, Taskhiri, and Turner (2020) had more reference trees and achieved similar DBH accuracy compared to that in this study, but the flights were piloted manually. Notably, the SfM-MVS approaches involved commercial lightweight drone systems, except He et al. (2025) where 360° camera was mounted as an additional payload to heavier LiDAR-based custom drone.

The most accurate under-canopy LiDAR-based DBH estimates were presented by

Hyypä et al. (2020a), achieving an RMSE of 0.6 cm (2.3 %) and bias of 0.34 cm (1.3 %) and 1.1 cm (3.5 %) and 0.12 cm (0.4 %) in two sparse forest plots. However, their system weighed around 10 kg and was piloted manually.

Autonomously operating under-canopy LiDAR-based drones were utilized in the studies by Muhojoki et al. (2024), Liang et al. (2024), and Cheng et al. (2024). While the commercial Hovermap drone system utilized in Muhojoki et al. (2024) achieved the lowest RMSE of these, the system was able to fly only in sparse and clean forests due to its size. The automated under-canopy UAV Lidar system by Liang et al. (2024) weighed 5 kg and provided an RMSE of 4.48 cm (21.37 %) and bias of 5.01 (14.91 %) at best. The autonomous system utilized in Cheng et al. (2024) weighed 4.2 kg and provided an RMSE of 3.8 cm (12.8 %) with the data collected in autonomous flight mode. The same LiDAR-based drone platform was used in studies by Prabhu et al. (2024) and He et al. (2025), but based on the articles, it seems that data collecting flights were performed in manual flight mode in these studies. Prabhu et al. (2024) reported RMSE of 1.67 cm (7.42 %) with LiDAR data, and He et al. (2025) reported median relative error of 11.5 % with photogrammetric point clouds from 360° camera data.

In summary, the highest accuracy levels were obtained with the relatively heavy ULS systems operated in sparse forest environments or in environments with few reference trees. Miniaturized lightweight sensors were used in the studies by Shimabuku, Konoshima, and Ota (2023), Krisanski, Taskhiri, and Turner (2020), Kuželka and Surovỳ (2018), Prabhu et al. (2024), Cheng et al. (2024), He et al. (2025), and Liang et al. (2024), though the LiDAR-based systems (Prabhu et al. 2024; Cheng et al. 2024; He et al. 2025; Liang et al. 2024) were still considerably heavier and larger than the camera-based drone systems. From these, only studies by Shimabuku, Konoshima, and Ota (2023), Cheng et al. (2024), and Liang et al. (2024) reported flights with a high level of automation, and LiDAR-based flights in Cheng et al. (2024) and Liang et al. (2024) were the only ones where the systems were able to fly without commands from the pilot during the flight. Considering the complexity of the environments, the density of the forest in Liang et al. (2024) (1000 trees/ha) was between the forests in this study (650 and 2000 trees/ha). The natural-like subtropical forest in Shimabuku, Konoshima, and Ota (2023) had seven trees in 5 m × 5 m area, leading to a density of 2000 trees/ha, but the test plot had minimal size. In Cheng et al. (2024), the forest density was not reported.

The approach proposed in this study, camera-based autonomous under-canopy flight and photogrammetric point cloud processing from low-cost onboard stereo camera data, yielded a similar level of estimation accuracy to most of the manually piloted UAV SfM-MVS systems (Kuželka and Surovỳ 2018; Krisanski, Taskhiri, and Turner 2020; He et al. 2025). Compared to the studies with LiDAR-based autonomous UAV collection, the accuracy was higher than in Liang et al. (2024) and similar than in Cheng et al. (2024) even without any GCPs. However, the system utilized in Cheng et al. (2024) has yielded slightly better accuracy with manually piloted flights (Cheng et al. 2024; Prabhu et al. 2024), suggesting that their LiDAR-based system has the potential for higher estimation accuracy by optimizing the autonomous flight trajectories.

Although the estimation accuracy obtained in this study was in line with most of the relevant studies even without any GCPs, the reconstruction quality (completeness and RMSE) can be further improved with GCPs.

Based on the previous, it can be concluded that camera-based autonomous miniaturized drones hold the potential to become a practical tool in forest parameter estimation. The potential estimation accuracy with low-cost stereo-cameras is near to the quality of small LiDARs suitable for miniaturized drones, but the weight and the price of

the sensor are considerably lower. This allows the building of smaller platforms capable of flying in denser forests, as well as reduces the cost of the system.

### 5.3. *Potential improvements and future work*

The empirical evaluation of the system revealed areas for improvement, which can inform further development toward a practical tool for operational forest measurements.

The reliability of navigation and the smoothness of the trajectory could be further improved by investigating alternative camera systems and image processing methods (e.g., image super-resolution) with a better capability of detecting thin branches. Blindsides in the obstacle avoidance map could be tackled either by sensors with 360° FOV (e.g., 360° camera or multi-camera system) or storing historical data to occupancy grid maps in addition to the currently visible area.

The virtual floor and ceiling of Ego-planner-V2 (Zhou et al. 2022) are also defined as static with respect to the takeoff location of the drone, limiting the low-altitude flying to relatively flat areas. To comprehensively map uneven forest plots, the altitude limits should be modified to be dynamic and concerning the local terrain level.

Drift compensation remains an important objective for future development. Initial loop closure tests yielded promising results, and future developments could assess the approach using block flights with a lawnmower pattern. In addition to the loop closures, the error in the position estimate could potentially be further reduced by fusing GNSS data to the VIO estimate. The potential methods for GNSS-Fusion include using the global fusion features in VINS-Fusion (Qin et al. 2019a) or replacing VINS-Fusion with another method fusing GNSS-data and VIO, e.g. GVINS (Cao, Lu, and Shen 2022). Even though the dense forest canopy blocks the GNSS signals, during long-term operations, the drone could receive corrections to the position estimate in the open areas while relying on the VIO estimate in denser parts of the forests.

It is also notable that the rigorous photogrammetric post-processing effectively compensated for the systematic errors. While the real-time trajectory error was 50 cm, the post-processed 3D error was approximately 11 cm without any GCPs. Therefore, for applications relying on post-processing, drift is unlikely to present significant challenges.

In this study, the performed flight paths were straight flights through the sample plots, and the DBH estimation was performed only for the tree trunks recorded during that path. For more comprehensive forest characterization, the trajectory should cover the whole test plot and observe the trees from multiple sides. Reconstructing the tree trunk from multiple sides instead of only one side could possibly also reduce the higher DBH estimation error obtained with the trees with large diameters. The global path covering the whole test plot could be implemented either with a simple waypoint generation algorithm as Liang et al. (2024) or with more advanced exploration methods such as proposed by Zhou et al. (2021a) or Cieslewski, Kaufmann, and Scaramuzza (2017). Another way to achieve area coverage would be utilizing a swarm of drones as in the original article by Zhou et al. (2022). Furthermore, recent exploration algorithms (Zhou, Xu, and Shen 2023)(Bartolomei, Teixeira, and Chli 2023) are able to utilize drone swarms to further improve and speed up the area coverage.

While this study focused on demonstrating the potential for forest characteristics estimation through DBH estimation and tree detection, the scope of data collection extends well beyond these applications. Including an additional lightweight camera pointing upwards would enable a more comprehensive reconstruction of the tree trunks to perform also stem curve estimation based on the point clouds. With the developed camera-based

prototype, data collection extends beyond point clouds to encompass applications such as image-based mapping and object detection. This opens up a variety of potential uses, including classifying and counting tree species and other vegetation, as well as monitoring bark damages caused by insect pests.

The prototype also opens possibilities for research of real-time forest characteristics analysis. In this study, the point clouds were obtained through post-processing. However, the onboard Intel Realsense D435 camera is also capable of generating 3D point clouds in real time. Additionally, image-based object detection can be performed in real-time, e.g., with YOLO (Redmon et al. 2016). While only computationally light analysis can be conducted on the onboard computer, real-time analysis with higher computational burden could be achieved through a remote computer or cloud service via an Internet connection.

## Acknowledgements

This research was funded by the Research Council of Finland within projects 'Learning techniques for autonomous drone based hyperspectral analysis of forest vegetation' (decision no. 357380), Fireman (decision no. 346710), and the Research Council of Finland Flagship Forest–Human–Machine Interplay—Building Resilience, Redefining Value Networks and Enabling Meaningful Experiences (UNITE) (decision no. 357908).

## Declaration of Competing Interest

The authors declare that they have no known competing financial interests or personal relationships that could have appeared to influence the work reported in this article.

## Data Availability Statement

Part of the data recorded during the field tests is available from the corresponding author upon reasonable request.

## References

- Ahmad, Afzal, Daniel Bonilla Licea, Giuseppe Silano, Tomas Baca, and Martin Saska. 2022. "PACNav: A collective navigation approach for UAV swarms deprived of communication and external localization." *Bioinspiration & Biomimetics* <https://doi.org/10.1088/1748-3190/ac98e6>.
- Balenović, Ivan, Xinlian Liang, Luka Jurjević, Juha Hyypä, Ante Seletković, and Antero Kukko. 2021. "Hand-held personal laser scanning—current status and perspectives for forest inventory application." *Croatian Journal of Forest Engineering: Journal for Theory and Application of Forestry Engineering* 42 (1): 165–183.
- Bartolomei, Luca, Lucas Teixeira, and Margarita Chli. 2023. "Fast Multi-UAV Decentralized Exploration of Forests." *IEEE Robotics and Automation Letters* 8 (9): 5576–5583. <https://doi.org/10.1109/LRA.2023.3296037>.
- Bauwens, Sébastien, Harm Bartholomeus, Kim Calders, and Philippe Lejeune. 2016. "Forest inventory with terrestrial LiDAR: A comparison of static and hand-held mobile laser scanning." *Forests* 7 (6): 127.

- Bienert, A, S Scheller, E Keane, F Mohan, and C Nugent. 2007. “Tree detection and diameter estimations by analysis of forest terrestrial laserscanner point clouds.” In *ISPRS workshop on laser scanning*, Vol. 36, 50–55. Citeseer.
- Bienert, Anne, Louis Georgi, Matthias Kunz, Hans-Gerd Maas, and Goddert Von Oheimb. 2018. “Comparison and combination of mobile and terrestrial laser scanning for natural forest inventories.” *Forests* 9 (7): 395.
- Brede, Benjamin, Alvaro Lau, Harm M Bartholomeus, and Lammert Kooistra. 2017. “Comparing RIEGL RiCOPTER UAV LiDAR derived canopy height and DBH with terrestrial LiDAR.” *Sensors* 17 (10): 2371.
- Cabo, Carlos, Susana Del Pozo, Pablo Rodríguez-González, Celestino Ordóñez, and Diego González-Aguilera. 2018. “Comparing terrestrial laser scanning (TLS) and wearable laser scanning (WLS) for individual tree modeling at plot level.” *Remote Sensing* 10 (4): 540.
- Calonder, Michael, Vincent Lepetit, Christoph Strecha, and Pascal Fua. 2010. “BRIEF: Binary Robust Independent Elementary Features.” In *Computer Vision – ECCV 2010*, edited by Kostas Daniilidis, Petros Maragos, and Nikos Paragios, Berlin, Heidelberg, 778–792. Springer Berlin Heidelberg.
- Campos-Macías, Leobardo, Rodrigo Aldana-López, Rafael de la Guardia, José I Parra-Vilchis, and David Gómez-Gutiérrez. 2021. “Autonomous navigation of MAVs in unknown cluttered environments.” *Journal of Field Robotics* 38 (2): 307–326. <https://doi.org/doi.org/10.1002/rob.21959>.
- Cao, Shaozu, Xiuyuan Lu, and Shaojie Shen. 2022. “GVINS: Tightly Coupled GNSS–Visual–Inertial Fusion for Smooth and Consistent State Estimation.” *IEEE Transactions on Robotics* 38 (4): 2004–2021. <https://doi.org/10.1109/TRO.2021.3133730>.
- Chen, Shilin, Haiyang Liu, Zhongke Feng, Chaoyong Shen, and Panpan Chen. 2019. “Applicability of personal laser scanning in forestry inventory.” *PLoS One* 14 (2): e0211392.
- Chen, Steven W., Guilherme V. Nardari, Elijah S. Lee, Chao Qu, Xu Liu, Roseli Ap. Francelin Romero, and Vijay Kumar. 2020. “SLOAM: Semantic Lidar Odometry and Mapping for Forest Inventory.” *IEEE Robotics and Automation Letters* 5 (2): 612–619. <https://doi.org/10.1109/LRA.2019.2963823>.
- Cheng, Derek, Fernando Cladera, Ankit Prabhu, Xu Liu, Alan Zhu, P. Corey Green, Reza Ehsani, Pratik Chaudhari, and Vijay Kumar. 2024. “TreeScope: An Agricultural Robotics Dataset for LiDAR-Based Mapping of Trees in Forests and Orchards.” In *2024 IEEE International Conference on Robotics and Automation (ICRA)*, 14860–14866.
- Chisholm, Ryan A, Jinqiang Cui, Shawn KY Lum, and Ben M Chen. 2013. “UAV LiDAR for below-canopy forest surveys.” *Journal of Unmanned Vehicle Systems* 1 (01): 61–68.
- Cieslewski, Titus, Elia Kaufmann, and Davide Scaramuzza. 2017. “Rapid exploration with multi-rotors: A frontier selection method for high speed flight.” In *2017 IEEE/RSJ International Conference on Intelligent Robots and Systems (IROS)*, 2135–2142.
- Ester, Martin, Hans-Peter Kriegel, Jörg Sander, and Xiaowei Xu. 1996. “A density-based algorithm for discovering clusters in large spatial databases with noise.” In *Kdd*, Vol. 96, 226–231.
- ETH Zürich Autonomous Systems Lab. 2023. “kalibr - IMU Noise Model.” ETH Zürich. <https://github.com/ethz-asl/kalibr/wiki/IMU-Noise-Model>. Accessed: 2024-05-27.
- Feng, Baokun, Sheng Nie, Cheng Wang, Xiaohuan Xi, Jinliang Wang, Guoqing Zhou, and Haoyu Wang. 2022. “Exploring the potential of UAV LiDAR data for trunk point extraction and direct DBH measurement.” *Remote Sensing* 14 (12): 2753.
- Forsman, Mona, Johan Holmgren, and Kenneth Olofsson. 2016. “Tree stem diameter estimation from mobile laser scanning using line-wise intensity-based clustering.” *Forests* 7 (9): 206.
- Furgale, Paul, Timothy D. Barfoot, and Gabe Sibley. 2012. “Continuous-time batch estimation using temporal basis functions.” In *2012 IEEE International Conference on Robotics and Automation*, 2088–2095.
- Furgale, Paul, Joern Rehder, and Roland Siegwart. 2013. “Unified temporal and spatial calibration for multi-sensor systems.” In *2013 IEEE/RSJ International Conference on Intelligent*

- Robots and Systems*, 1280–1286.
- Galvez-López, Dorian, and Juan D. Tardos. 2012. “Bags of Binary Words for Fast Place Recognition in Image Sequences.” *IEEE Transactions on Robotics* 28 (5): 1188–1197. <https://doi.org/10.1109/TRO.2012.2197158>.
- Gao, Qiang, and Jiangming Kan. 2022. “Automatic Forest DBH Measurement Based on Structure from Motion Photogrammetry.” *Remote Sensing* 14 (9). <https://doi.org/10.3390/rs14092064>, <https://www.mdpi.com/2072-4292/14/9/2064>.
- He, Siming, Zachary Osman, Fernando Cladera, Dexter Ong, Nitant Rai, Patrick Corey Green, Vijay Kumar, and Pratik Chaudhari. 2025. “Estimating the Diameter at Breast Height of Trees in a Forest With a Single 360 Camera.” *arXiv preprint arXiv:2505.03093*.
- Hyypä, Eric, Juha Hyypä, Teemu Hakala, Antero Kukko, Michael A Wulder, Joanne C White, Jiri Pyörälä, et al. 2020a. “Under-canopy UAV laser scanning for accurate forest field measurements.” *ISPRS Journal of Photogrammetry and Remote Sensing* 164: 41–60.
- Hyypä, Eric, Antero Kukko, Harri Kaartinen, Xiaowei Yu, Jesse Muhojoki, Teemu Hakala, and Juha Hyypä. 2022. “Direct and automatic measurements of stem curve and volume using a high-resolution airborne laser scanning system.” *Science of Remote Sensing* 5: 100050.
- Hyypä, Eric, Antero Kukko, Risto Kaijaluoto, Joanne C White, Michael A Wulder, Jiri Pyörälä, Xinlian Liang, et al. 2020b. “Accurate derivation of stem curve and volume using backpack mobile laser scanning.” *ISPRS Journal of Photogrammetry and Remote Sensing* 161: 246–262.
- Hyypä, Eric, Xiaowei Yu, Harri Kaartinen, Teemu Hakala, Antero Kukko, Mikko Vastaranta, and Juha Hyypä. 2020c. “Comparison of backpack, handheld, under-canopy UAV, and above-canopy UAV laser scanning for field reference data collection in boreal forests.” *Remote Sensing* 12 (20): 3327.
- Intel Realsense Development Team. 2023. “Depth Camera D435.” Intel Corporation. <https://www.intelrealsense.com/depth-camera-d435/>.
- Karjalainen, V., T. Hakala, A. George, N. Koivumäki, J. Suomalainen, and E. Honkavaara. 2023. “A DRONE SYSTEM FOR AUTONOMOUS MAPPING FLIGHTS INSIDE A FOREST – A FEASIBILITY STUDY AND FIRST RESULTS.” *The International Archives of the Photogrammetry, Remote Sensing and Spatial Information Sciences XLVIII-1/W2-2023*: 597–603. <https://doi.org/10.5194/isprs-archives-XLVIII-1-W2-2023-597-2023>.
- Keselman, Leonid, John Iselin Woodfill, Anders Grunnet-Jepsen, and Achintya Bhowmik. 2017. “Intel(R) RealSense(TM) Stereoscopic Depth Cameras.” In *2017 IEEE Conference on Computer Vision and Pattern Recognition Workshops (CVPRW)*, 1267–1276.
- Krisanski, Sean, Mohammad Sadegh Taskhiri, and Paul Turner. 2020. “Enhancing Methods for Under-Canopy Unmanned Aircraft System Based Photogrammetry in Complex Forests for Tree Diameter Measurement.” *Remote Sensing* 12 (10). <https://doi.org/10.3390/rs12101652>, <https://www.mdpi.com/2072-4292/12/10/1652>.
- Kuan, Yau Weng, Ng Oon Ee, and Lee Sze Wei. 2019. “Comparative Study of Intel R200, Kinect v2, and Primesense RGB-D Sensors Performance Outdoors.” *IEEE Sensors Journal* 19 (19): 8741–8750. <https://doi.org/10.1109/JSEN.2019.2920976>.
- Kuželka, Karel, Martin Slavík, and Peter Surový. 2020. “Very high density point clouds from UAV laser scanning for automatic tree stem detection and direct diameter measurement.” *Remote Sensing* 12 (8): 1236.
- Kuželka, Karel, and Peter Surový. 2018. “Mapping forest structure using UAS inside flight capabilities.” *Sensors* 18 (7): 2245.
- Laasasenaho, Jouko. 1982. *Taper curve and volume functions for pine, spruce and birch*.
- Leica Geosystems. 2020. “Leica Nova TS60 Data sheet.” <https://leica-geosystems.com/products/total-stations/robotic-total-stations/leica-nova-ts60/>.
- Liang, Xinlian, Anttoni Jaakkola, Yunsheng Wang, Juha Hyypä, Eija Honkavaara, Jingbin Liu, and Harri Kaartinen. 2014a. “The use of a hand-held camera for individual tree 3D mapping in forest sample plots.” *Remote Sensing* 6 (7): 6587–6603.
- Liang, Xinlian, Antero Kukko, Juha Hyypä, Matti Lehtomäki, Jiri Pyörälä, Xiaowei Yu, Harri Kaartinen, Anttoni Jaakkola, and Yunsheng Wang. 2018. “In-situ measurements from

- mobile platforms: An emerging approach to address the old challenges associated with forest inventories.” *ISPRS Journal of Photogrammetry and Remote Sensing* 143: 97–107.
- Liang, Xinlian, Antero Kukko, Harri Kaartinen, Juha Hyypä, Xiaowei Yu, Anttoni Jaakkola, and Yunsheng Wang. 2014b. “Possibilities of a personal laser scanning system for forest mapping and ecosystem services.” *Sensors* 14 (1): 1228–1248.
- Liang, Xinlian, Yunsheng Wang, Jiri Pyörälä, Matti Lehtomäki, Xiaowei Yu, Harri Kaartinen, Antero Kukko, et al. 2019. “Forest in situ observations using unmanned aerial vehicle as an alternative of terrestrial measurements.” *Forest ecosystems* 6: 1–16.
- Liang, Xinlian, Haiyun Yao, Hanwen Qi, and Xiaochen Wang. 2024. “Forest in situ observations through a fully automated under-canopy unmanned aerial vehicle.” *Geo-spatial Information Science* 1–17.
- Liu, Wenyi, Yunfan Ren, and Fu Zhang. 2024. “Integrated Planning and Control for Quadrotor Navigation in Presence of Suddenly Appearing Objects and Disturbances.” *IEEE Robotics and Automation Letters* 9 (1): 899–906. <https://doi.org/10.1109/LRA.2023.3311358>.
- Liu, Xu, Guilherme V. Nardari, Fernando Cladera Ojeda, Yuezhan Tao, Alex Zhou, Thomas Donnelly, Chao Qu, et al. 2022. “Large-Scale Autonomous Flight With Real-Time Semantic SLAM Under Dense Forest Canopy.” *IEEE Robotics and Automation Letters* 7 (2): 5512–5519. <https://doi.org/doi.org/10.1109/LRA.2022.3154047>.
- Loquercio, Antonio, Elia Kaufmann, René Ranftl, Matthias Müller, Vladlen Koltun, and Davide Scaramuzza. 2021. “Learning high-speed flight in the wild.” *Science Robotics* 6 (59): eabg5810. <https://doi.org/doi.org/10.1126/scirobotics.abg5810>.
- Lucas, Bruce D, and Takeo Kanade. 1981. “An iterative image registration technique with an application to stereo vision.” In *IJCAI’81: 7th international joint conference on Artificial intelligence*, Vol. 2, 674–679.
- Marselis, Suzanne M, Marta Yebra, Tom Jovanovic, and Albert IJM van Dijk. 2016. “Deriving comprehensive forest structure information from mobile laser scanning observations using automated point cloud classification.” *Environmental modelling & software* 82: 142–151.
- Maye, Jérôme, Paul Furgale, and Roland Siegwart. 2013. “Self-supervised calibration for robotic systems.” In *2013 IEEE Intelligent Vehicles Symposium (IV)*, 473–480.
- Mellinger, Daniel, and Vijay Kumar. 2011. “Minimum snap trajectory generation and control for quadrotors.” In *2011 IEEE International Conference on Robotics and Automation*, 2520–2525.
- Metashape Development Team. 2021. “Agisoft Metashape Software, Version 1.7.” Agisoft LLC. <https://www.agisoft.com/downloads/installer/>.
- Mokroš, Martin, Jozef Východík, Julián Tomašík, Alžbeta Grznárová, Peter Valent, Martin Slavík, and Ján Merganič. 2018. “High precision individual tree diameter and perimeter estimation from close-range photogrammetry.” *Forests* 9 (11): 696.
- Moravec, Hans, and Alberto Elfes. 1985. “High resolution maps from wide angle sonar.” In *Proceedings. 1985 IEEE international conference on robotics and automation*, Vol. 2, 116–121. IEEE.
- Muhojoki, Jesse, Daniella Tavi, Eric Hyypä, Matti Lehtomäki, Tamás Faitli, Harri Kaartinen, Antero Kukko, Teemu Hakala, and Juha Hyypä. 2024. “Benchmarking Under- and Above-Canopy Laser Scanning Solutions for Deriving Stem Curve and Volume in Easy and Difficult Boreal Forest Conditions.” *Remote Sensing* 16 (10). <https://doi.org/10.3390/rs16101721>, <https://www.mdpi.com/2072-4292/16/10/1721>.
- Nguyen, Huan, Rasmus Andersen, Evangelos Boukas, and Kostas Alexis. 2023. “Uncertainty-aware visually-attentive navigation using deep neural networks.” *The International Journal of Robotics Research* 0 (0): 02783649231218720. <https://doi.org/10.1177/02783649231218720>.
- Olson, Edwin. 2011. “AprilTag: A robust and flexible visual fiducial system.” In *2011 IEEE International Conference on Robotics and Automation*, 3400–3407.
- Oxford Dynamic Robot Systems Group. 2022. “Allan Variance ROS.” University of Oxford. [https://github.com/ori-drs/allan\\_variance\\_ros](https://github.com/ori-drs/allan_variance_ros).
- Piermattei, Livia, Wilfried Karel, Di Wang, Martin Wieser, Martin Mokroš, Peter Surový,

- Milan Koreň, Julián Tomašík, Norbert Pfeifer, and Markus Hollaus. 2019. “Terrestrial structure from motion photogrammetry for deriving forest inventory data.” *Remote Sensing* 11 (8): 950.
- Prabhu, Ankit, Xu Liu, Igor Spasojevic, Yuwei Wu, Yifei Shao, Dexter Ong, Jiuzhou Lei, Patrick Corey Green, Pratik Chaudhari, and Vijay Kumar. 2024. “UAVs for forestry: Metric-semantic mapping and diameter estimation with autonomous aerial robots.” *Mechanical Systems and Signal Processing* 208: 111050. <https://doi.org/https://doi.org/10.1016/j.ymssp.2023.111050>, <https://www.sciencedirect.com/science/article/pii/S0888327023009585>.
- Puliti, Stefano, Hans Ole Ørka, Terje Gobakken, and Erik Næsset. 2015. “Inventory of Small Forest Areas Using an Unmanned Aerial System.” *Remote Sensing* 7 (8): 9632–9654. <https://doi.org/10.3390/rs70809632>, <https://www.mdpi.com/2072-4292/7/8/9632>.
- PX4 Community. 2023. “PX4-Autopilot, Version 1.14.0.” <https://github.com/PX4/PX4-Autopilot>.
- Qin, Tong, Shaozu Cao, Jie Pan, and Shaojie Shen. 2019a. “A General Optimization-based Framework for Global Pose Estimation with Multiple Sensors.” *arXiv preprint arXiv:1901.03642* <https://doi.org/doi.org/10.48550/arXiv.1901.03642>.
- Qin, Tong, Peiliang Li, and Shaojie Shen. 2018. “Vins-mono: A robust and versatile monocular visual-inertial state estimator.” *IEEE Transactions on Robotics* 34 (4): 1004–1020. <https://doi.org/doi.org/10.1109/TRO.2018.2853729>.
- Qin, Tong, Jie Pan, Shaozu Cao, and Shaojie Shen. 2019b. “A general optimization-based framework for local odometry estimation with multiple sensors.” *arXiv preprint arXiv:1901.03638* <https://doi.org/doi.org/10.48550/arXiv.1901.03638>.
- Qin, Tong, and Shaojie Shen. 2018. “Online Temporal Calibration for Monocular Visual-Inertial Systems.” In *2018 IEEE/RSJ International Conference on Intelligent Robots and Systems (IROS)*, 3662–3669.
- Quigley, Morgan, Josh Faust, Tully Foote, Jeremy Leibs, et al. 2009. “ROS: an open-source Robot Operating System.” In *Proc. of the IEEE Intl. Conf. on Robotics and Automation (ICRA), Workshop on Open Source Robotics*, Kobe, Japan, May.
- Reddy Cenkeramaddi, Linga, Jyoti Bhatia, Ajit Jha, Santosh Kumar Vishkarma, and J. Soumya. 2020. “A Survey on Sensors for Autonomous Systems.” In *2020 15th IEEE Conference on Industrial Electronics and Applications (ICIEA)*, 1182–1187.
- Redmon, Joseph, Santosh Divvala, Ross Girshick, and Ali Farhadi. 2016. “You Only Look Once: Unified, Real-Time Object Detection.” In *Proceedings of the IEEE Conference on Computer Vision and Pattern Recognition (CVPR)*, June.
- Ren, Yunfan, Fangcheng Zhu, Wenyi Liu, Zhepei Wang, Yi Lin, Fei Gao, and Fu Zhang. 2022. “Bubble Planner: Planning High-speed Smooth Quadrotor Trajectories using Receding Corridors.” In *2022 IEEE/RSJ International Conference on Intelligent Robots and Systems (IROS)*, 6332–6339.
- Ryding, Joseph, Emily Williams, Martin J Smith, and Markus P Eichhorn. 2015. “Assessing handheld mobile laser scanners for forest surveys.” *Remote sensing* 7 (1): 1095–1111.
- Schubert, F. M., B. H. Fleury, P. Robertson, R. Prieto-Cerdeira, A. Steingass, and A. Lehner. 2010. “Modeling of multipath propagation components caused by trees and forests.” In *Proceedings of the Fourth European Conference on Antennas and Propagation*, 1–5.
- Shi, Jianbo, and Tomasi. 1994. “Good features to track.” In *1994 Proceedings of IEEE Conference on Computer Vision and Pattern Recognition*, 593–600.
- Shimabuku, Fu, Masashi Konoshima, and Ikuo Ota. 2023. “Diameter and stem volume estimation based on under canopy UAV-SfM-MVS survey approach in subtropical forest of Okinawa Island, Japan.” *FORMATH* 22: 22–004.
- Sturm, Jürgen, Nikolas Engelhard, Felix Endres, Wolfram Burgard, and Daniel Cremers. 2012. “A benchmark for the evaluation of RGB-D SLAM systems.” In *2012 IEEE/RSJ International Conference on Intelligent Robots and Systems*, 573–580.
- Surovỳ, Peter, Atsushi Yoshimoto, and Dimitrios Panagiotidis. 2016. “Accuracy of reconstruction of the tree stem surface using terrestrial close-range photogrammetry.” *Remote Sensing*

- 8 (2): 123.
- Tuominen, Sakari, Andras Balazs, Eija Honkavaara, Ilkka Pölönen, Heikki Saari, Teemu Hakala, and Niko Viljanen. 2017. “Hyperspectral UAV-imagery and photogrammetric canopy height model in estimating forest stand variables.” *Silva Fennica* 51 (5).
- Umeyama, S. 1991. “Least-squares estimation of transformation parameters between two point patterns.” *IEEE Transactions on Pattern Analysis and Machine Intelligence* 13 (4): 376–380. <https://doi.org/10.1109/34.88573>.
- Usenko, Vladyslav, Lukas von Stumberg, Andrej Pangercic, and Daniel Cremers. 2017. “Real-time trajectory replanning for MAVs using uniform B-splines and a 3D circular buffer.” In *2017 IEEE/RSJ International Conference on Intelligent Robots and Systems (IROS)*, 215–222.
- Vandendaele, Bastien, Richard A Fournier, Udayalakshmi Vepakomma, Gaetan Pelletier, Philippe Lejeune, and Olivier Martin-Ducup. 2021. “Estimation of northern hardwood forest inventory attributes using UAV laser scanning (ULS): Transferability of laser scanning methods and comparison of automated approaches at the tree-and stand-level.” *Remote Sensing* 13 (14): 2796.
- Viljanen, Niko, Eija Honkavaara, Roope Näsi, Teemu Hakala, Oiva Niemeläinen, and Jere Kaivosoja. 2018. “A Novel Machine Learning Method for Estimating Biomass of Grass Swards Using a Photogrammetric Canopy Height Model, Images and Vegetation Indices Captured by a Drone.” *Agriculture* 8 (5): 70. <https://doi.org/10.3390/agriculture8050070>.
- Wallace, Luke, Arko Lucieer, Zbyněk Malenovský, Darren Turner, and Petr Vopěnka. 2016. “Assessment of forest structure using two UAV techniques: A comparison of airborne laser scanning and structure from motion (SfM) point clouds.” *Forests* 7 (3): 62.
- Wang, Yunsheng, Antero Kukko, Eric Hyyppä, Teemu Hakala, Jiri Pyörälä, Matti Lehtomäki, Aimad El Issaoui, et al. 2021. “Seamless integration of above-and under-canopy unmanned aerial vehicle laser scanning for forest investigation.” *Forest Ecosystems* 8: 1–15.
- Wang, Yunsheng, Matti Lehtomäki, Xinlian Liang, Jiri Pyörälä, Antero Kukko, Anttoni Jaakkola, Jingbin Liu, Ziyi Feng, Ruizhi Chen, and Juha Hyyppä. 2019. “Is field-measured tree height as reliable as believed—A comparison study of tree height estimates from field measurement, airborne laser scanning and terrestrial laser scanning in a boreal forest.” *IS-PRS journal of photogrammetry and remote sensing* 147: 132–145.
- Wang, Zhepei, Xin Zhou, Chao Xu, and Fei Gao. 2022. “Geometrically constrained trajectory optimization for multicopters.” *IEEE Transactions on Robotics* 38 (5): 3259–3278. <https://doi.org/doi.org/10.1109/TRO.2022.3160022>.
- Wieser, Martin, Gottfried Mandlbürger, Markus Hollaus, Johannes Otepka, Philipp Glira, and Norbert Pfeifer. 2017. “A case study of UAS borne laser scanning for measurement of tree stem diameter.” *Remote Sensing* 9 (11): 1154.
- Xu, Zhuangzhi, Xin Shen, and Lin Cao. 2023. “Extraction of Forest Structural Parameters by the Comparison of Structure from Motion (SfM) and Backpack Laser Scanning (BLS) Point Clouds.” *Remote Sensing* 15: 2144. <https://doi.org/10.3390/rs15082144>.
- Ye, Ning, Louise van Leeuwen, and Panagiotis Nyktas. 2019. “Analysing the potential of UAV point cloud as input in quantitative structure modelling for assessment of woody biomass of single trees.” *International Journal of Applied Earth Observation and Geoinformation* 81: 47–57.
- Zhang, Zichao, and Davide Scaramuzza. 2018. “A Tutorial on Quantitative Trajectory Evaluation for Visual(-Inertial) Odometry.” In *2018 IEEE/RSJ International Conference on Intelligent Robots and Systems (IROS)*, 7244–7251.
- Zhou, Boyu, Hao Xu, and Shaojie Shen. 2023. “RACER: Rapid Collaborative Exploration With a Decentralized Multi-UAV System.” *IEEE Transactions on Robotics* 39 (3): 1816–1835. <https://doi.org/10.1109/TRO.2023.3236945>.
- Zhou, Boyu, Yichen Zhang, Xinyi Chen, and Shaojie Shen. 2021a. “FUEL: Fast UAV Exploration Using Incremental Frontier Structure and Hierarchical Planning.” *IEEE Robotics and Automation Letters* 6 (2): 779–786. <https://doi.org/10.1109/LRA.2021.3051563>.
- Zhou, Xin, Zhepei Wang, Hongkai Ye, Chao Xu, and Fei Gao. 2021b. “EGO-Planner: An

- ESDF-Free Gradient-Based Local Planner for Quadrotors.” *IEEE Robotics and Automation Letters* 6 (2): 478–485. <https://doi.org/10.1109/LRA.2020.3047728>.
- Zhou, Xin, Xiangyong Wen, Zhepei Wang, Yuman Gao, Haojia Li, Qianhao Wang, Tiankai Yang, et al. 2022. “Swarm of micro flying robots in the wild.” *Science Robotics* 7 (66): eabm5954. <https://doi.org/doi.org/10.1126/scirobotics.abm5954>.
- ZJU FAST Lab Team. 2022a. “EGO-Planner-v2.” Zhejiang University. <https://github.com/ZJU-FAST-Lab/EGO-Planner-v2>.
- ZJU FAST Lab Team. 2022b. “px4ctrl.” Zhejiang University. [https://github.com/ZJU-FAST-Lab/Fast-Drone-250/tree/master/src/realflight\\_modules/px4ctrl](https://github.com/ZJU-FAST-Lab/Fast-Drone-250/tree/master/src/realflight_modules/px4ctrl).